Hindawi
Advances in Civil Engineering
Volume 2022, Article ID 4644433, 24 pages
https://doi.org/10.1155/2022/4644433

*Research Article*

# Numerical Investigation of Textile Reinforced Cement Structural Stay-in-Place Formwork Designed as Beam-Column Joint Shear Reinforcement

**Negasa Desta,[1] Kabtamu Getachew ,[2] and Daba Geresu[1]**

[1]*Civil Engineering Department, College of Architecture and Civil Engineering, Addis Ababa Science and Technology University, Addis Ababa, Ethiopia*
[2]*Civil Engineering Department, Jimma Institute of Technology, Jimma University, Jimma, Ethiopia*

Correspondence should be addressed to Kabtamu Getachew; kabtamgetachew@gmail.com

Received 14 January 2022; Revised 13 April 2022; Accepted 20 May 2022; Published 30 June 2022

Academic Editor: Junqing Zuo



This study investigates the feasibility and structural performance of textile reinforced cement (TRC) stay-in-place (SiP) formwork designed as shear reinforcement for beam-column joints under monotonic loading through the nonlinear finite element package ABAQUS. This was achieved by conducting numerical analysis on 24 beam-column joints using different parameters that affect the joints' performance, including column axial load ratio, concrete compressive strength, beam tensile reinforcement ratio, joint shear reinforcement ratio, and thickness of TRC. The models were first calibrated to the results obtained from the experimental program of previous studies. The start of the yielding behavior of the composite beam-column (73 kN) corresponds well to the conventional beam-column joint (72 kN). A similar correlation can be observed at the ultimate load with only a 3.7% difference, 84 kN in the case of the composite beam-column joint and 81 kN in the case of the conventional beam-column joint. The findings of this investigation showed that a beam-column with a full steel stirrup and TRC SiP formwork as shear reinforcement at the joint exhibits similar yielding behavior, such that TRC SiP formwork can replace the full steel stirrup at the joint, as proved by comparison analysis. Furthermore, the numerical analysis results due to the effect of these essential parameters on the structural performance of the beam-column with TRC SiP formwork at the joint were also discussed.

## 1. Introduction

Due to the availability of steel and concrete, design knowledge, and extensive experience with their usage in practice, conventional reinforced concrete is widely used in the construction industry. However, the corrosion susceptibility of steel reinforcement, prolonged construction time, undesirable stresses in concrete components while removing formwork, and the high expense of construction owing to the putting and tying of reinforcement in conventional reinforced concrete have all become major engineering and economic problems. To solve problems associated with conventional RC, composite reinforced concrete with TRC SiP formwork has sparked a lot of attention in structural engineering research during the last few decades because of its superior physical and mechanical qualities, including corrosion resistance, low self-weight, high tensile strength, and fire resistance.

Structural SiP formwork is a type of formwork that is not removed after the concrete has been cast and serves as a formwork during the plastic stage of the concrete as well as reinforcement after the concrete has hardened. This improves problems associated with temporary formwork, eliminating undesirable stresses and the risk of damaging concrete while removing formwork [1]. The detailing mechanism provided by different design codes to increase the efficiency of the beam-column joint may lead to reinforcement congestion at the joint. To alleviate this problem,

the use of textile fiber cement may be an alternative to get the required design efficiency at the join with a limited number of shear reinforcements or without shear reinforcement. TRC SiP formwork can help us achieve our goals of faster construction, lower costs, and improved durability because it serves multiple functions as formwork, reinforcement, and a protective shell against corrosion, weathering, and chemicals [2]. They can also be designed as structural elements and could fully or partially replace the required reinforcement [3–5].

Many researchers have also studied the structural performance of beam-column joints due to the effect of different parameters. For instance, Allam et al. [6] carried out a numerical analysis on external reinforced concrete beam-column joints under monotonic loading and discovered that joint failure was caused by shear diagonal tension and that increasing the column axial load increased the beam tip ultimate load. In addition, an experimental study carried out on beam-column joints demonstrated that at the initial stages of loading, an increase in axial load enhances the shear capacity of the joint and reduces its ductility [7–9]. This finding contradicts [10,11], who concluded that the presence of axial stress had no effect on joint shear strength. With an increase in axial compression ratio in the core area, both the ductility and energy consumption of beam-column joints increase [12]. The test result obtained here is totally different from the result obtained by Yang et al. [13], in which ductility decreases with an increase in axial load ratio. The axial load value can influence the damage evolution and, as a result, the deformation capacity of beam-column joints. In fact, when compared to the joint tested under low axial load, the joint with higher axial load exhibits delayed vertical cracking at the beam-column interface [14].

Allam et al. [6] conducted analyses on beam-column joints and found that increasing the concrete strength improves the joint resistance by improving the load-bearing capacity. It was also discovered that there was a nonlinear relationship between concrete strength and ultimate load, which corresponded to the commonly observed nonlinear relationship between the axial compressive and shear strength of concrete. This contradicts a result obtained by Noguchi and Kashiwazaki [15], who concluded that the concrete compressive strength does not affect the maximum joint shear strength. Among the influence factors, concrete compressive strength had the most significant correlation with joint shear strength, and interestingly, it was higher for interior connections than for exterior connections [16].

Abdelwahed et al. [17] investigated numerically the behavior of inverted knee joints and found that the increase in the beam reinforcement percentage has a positive effect on the load-carrying capacity and the rate of strength degradation. A test carried out on the beam-column joint also showed that reinforcement ratio has a positive effect on shear strength [18]. Furthermore, an experimental study on reinforced concrete interior beam-column joints indicated that the joint stirrup reinforcement ratio had little influence on the ductility and shear strength of the joint. In addition, it has no influence on the strength and deformation of interior beam-column subassemblies [19]. This result conflicts with the result obtained by Kaung and Wong [20].

To improve the safety of existing RC frame buildings, the strength of beam-column joints must be increased so that strong column-weak beam behavior can be achieved. The various frequently used strengthening techniques involve steel plate bonding, concrete jacketing, and the use of composite materials like fiber reinforced polymer (FRP). The use of carbon fiber ropes as external strengthening reinforcement has been shown to be an efficient strengthening technique in terms of load carrying, stiffness, energy dissipation, and damage when compared to unstrengthened specimens [21]. The experimental study conducted by Maras and Kantarci [22] revealed that CFRP composites could be a viable alternative for greatly improving structural performance and providing appropriate and dependable solutions for long-term structures. Experimental test results also indicated that a reinforced UHPFRC beam-column joint has a higher initial cracking strength and shear carrying capacity [23]. Furthermore, compared to conventional reinforced beam-column joints, steel fiber reinforced beam-column joints have better ductility, load-carrying capacity, energy dissipation, and strength [24].

The key distinction between past research and this research is that most of the previous research was concentrated on the investigation of RC or steel jacketing, timber, and FRPs stay-in-place formwork, especially for the slab and beam. These techniques cause various difficulties in practical implementation at the joint, namely intensive labor, increased dimensions, corrosion protection, and fire resistance, and are relatively expensive. As a result, this research is being carried out to address a gap in knowledge about some of the disadvantages of commonly used materials, such as the durability of timber, the corrosion sensitivity of steel, fire resistance, and the cost of FRP. Proper design and detailing of the joint is important because RC connections are the most vulnerable elements during loading and can undergo shear failure in the joint. The work contained here is thus critical in addressing the technique of increasing the capacity of these zones by TRC with the goal of relocating potential plastic hinges from the joint to the beams or columns without debonding or rupture.

The results of this study are important to set the maximum design load value to be applied to the column and the tensile reinforcement ratios to be used in the beam. The results of the study are also significant in addressing the effectiveness of TRC in making components with a considerably smaller amount of material and a longer service life than conventional concrete, as well as in extending the life span of existing structures that are undergoing deterioration or need upgrading to withstand higher loads. The objective of this research is to investigate numerically the feasibility and performance of structural stay-in-place formwork made of TRC designed as shear reinforcement for beam-column joints, using different parameters known to affect the joints' performance, including column axial load ratio, concrete compressive strength, beam tensile reinforcement ratio, joint shear reinforcement ratio, and thickness of TRC.

## 2. Finite Element Modeling

In this study, the ABAQUS finite element program was used to simulate the behavior of the beam-column joint. Because of its user-friendly interface and support for parametric modeling, ABAQUS was chosen for this simulation. In order to properly simulate the behavior of a beam-column joint, geometrical and material nonlinearities are taken into account. The concrete damage plasticity (CDP) model is chosen and introduced to the numerical model among constitutive models defining concrete's nonlinear behavior as a quasi-brittle material available in ABAQUS, such as smeared and brittle cracking models. The models were first calibrated to the results obtained from the experimental programs of previous researchers. In this study, the valuable data and observations from experimental results of the first base control and referential specimen, from Mahmoud et al. [25], were chosen, and the NLFE software ABAQUS was utilized for numerical simulation and modeling to trace the response of the beam-column.

*2.1. Model Geometry.* The model has a 0.9-m long extruded beam with cross-sectional dimensions of $0.2 \times 0.3$ m. The column has a cross section of $0.2 \times 0.3$ m and a total length of 2.3 m divided into two equal parts, namely lower and upper. The main steel reinforcement of the beam was three bars of 16 mm in diameter, while the secondary steel reinforcement was two bars of 12 mm in diameter. The column, on the other hand, was reinforced with four bars of 16 mm in diameter at each corner of the column cross section. The stirrups for both the beam and the column were mild steel bars of 8 mm in diameter and spaced every 0.1 m and 0.15 m for the beam and the column, respectively. Geometry and reinforcement details of the beam-column joints are shown in Figure 1.

The thickness of TRC is calculated such that the composite beam-column joint is capable of bearing the same shear loads in the permanent state as the conventional beam-column at the joint. The required thickness of TRC to be equivalent to a steel stirrup in order to fulfill shear requirements is only 0.003 m and is shown at the beam-column joint in Figure 2.

*2.2. Material Properties.* The concrete used was normal concrete with target strength of 25 MPa. Both the beam and the columns were reinforced longitudinally with deformed bars with yield strength of 400 MPa, while the stirrups were ordinary mild steel with yield strength of 240 MPa. Both types of reinforcement had a modulus of elasticity of 200 MPa and a Poisson ratio of 0.3. The Young modulus of the textile reinforced cement is 18 GPa, and the Poisson ratio is 0.3. It also has 60 MPa and 80 MPa tensile and compressive strengths, respectively.

*2.3. Loading and Boundary Conditions.* A compression load equal to 200 kN, simulating the load in a real structure, was first applied to the column before the beam was loaded.

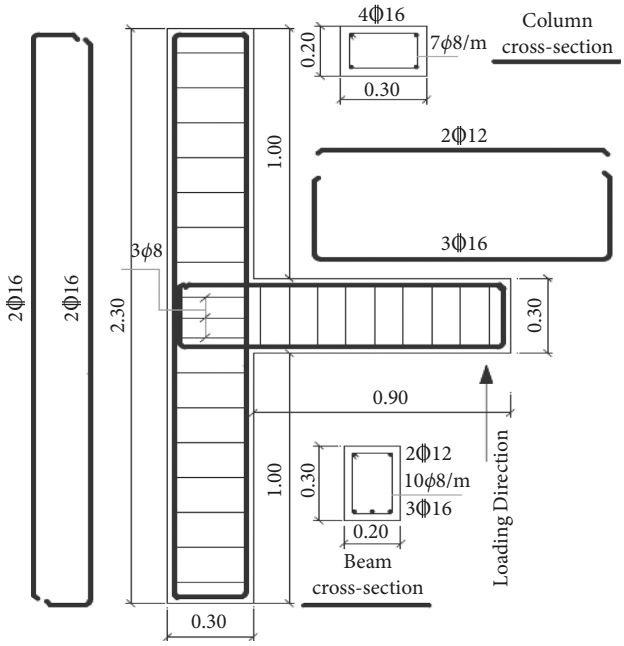


Figure 1: Model geometry and reinforcement detailing [25].

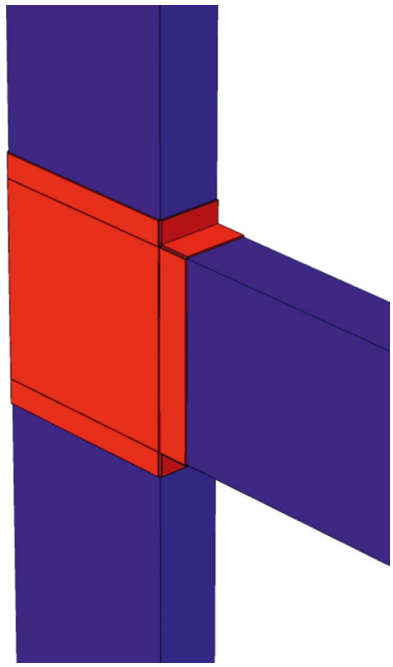

Figure 2: Textile reinforced cement model geometry at the joint.

Then, the beam was kept as a cantilever and monotonic loading was applied to it at 0.9 m from the face of the column in several steps up to failure. The specimens were considered hinged at both column ends (Figure 3). The tested specimens were symmetrical with respect to the vertical plane crossing through the beam/column width. In addition to geometric symmetry, the applied load and resulting failure modes were also symmetrical. Hence, the symmetry was exploited to reduce the computational cost by modeling only half of the specimen and imposing appropriate symmetry boundary

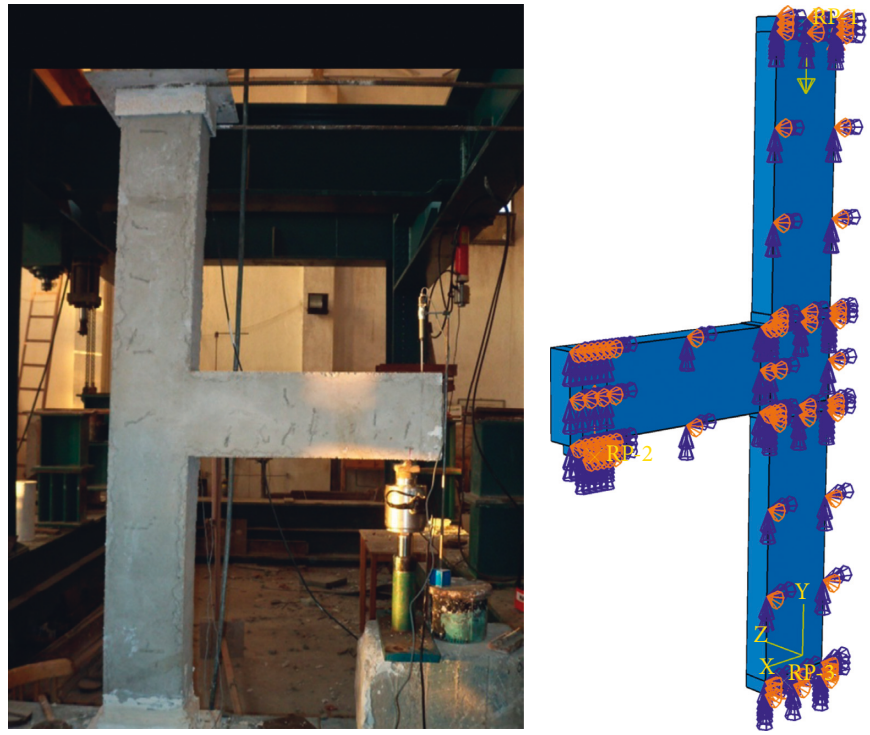


(a) (b)

Figure 3: Boundary conditions and loading: (a) test setup [25] and (b) finite element.

conditions. To simulate the boundary conditions of the test specimens during experimental testing, the column ends were restrained against movement to simulate pin supports at both ends, and the right support was restrained against movement in the $Z$-direction along the plane of symmetry.

*2.4. Mesh Sensitivity Study.* Meshing is the process of generating nodes and elements. Because matrices based on structured meshing are simple and quick to assemble, they were used for all of the solid elements in the models. Furthermore, the aspect ratios of solid elements were kept as close to one as possible, as high aspect ratio elements would affect the accuracy of the analysis. Mesh convergence studies were carried out to determine the best mesh size and material parameters for a close match with the experimentally observed response. Initially, three element sizes were used as a uniform mesh size: 0.025 m, 0.035 m, and 0.050 m. Figure 4 shows the comparison between experimental test results and different mesh sizes using a reduced integration element with eight nodes (C3D8R). The similarity of the curve in the FE analysis using the 0.025 m element size to that obtained by experiment suggested that the experimental observation and the prediction result from the FE analysis were in reasonably good agreement.

*2.5. Element Types and Material Modeling*

*2.5.1. Concrete.* The 8-node linear brick element with reduced integration (C3D8R) and hourglass control was chosen to model concrete throughout this study and is shown in Figure 5.

The FE model takes into account both elastic and inelastic concrete behavior. It is assumed that the concrete element is homogeneous and isotropic. A concrete damage plasticity (CDP) model is utilized in the study to define concrete material behavior in the inelastic range. The compressive and tensile stiffness recoveries are defined by the factors wt and wc, through the load reversal. The set values for these factors were as default, that is, wt = 0 and wc = 1. The degradation of the elastic stiffness is characterized by two damage variables, dt and dc. The evolution of concrete damage, both in compression and tension, was linked to the corresponding inelastic strain, using

$$d = 1 - \frac{\sigma}{\sigma_{\max}}. \quad (1)$$

To generalize concrete uniaxial stress-strain features to the 3D stress space, the CDP model requires various input parameters. The CDPM parameters shown in Table 1 are calibrated and used throughout this study.

Many models have been proposed to capture the nonlinear behavior of concrete in compression and tension by transverse reinforcement. For the scope of this study, the Hognestad model (Figure 6) and the Belarbi and Hsu model (Figure 7) were selected. This is because the models are quite capable of capturing the behavior of the concrete under compression and tension, respectively. In addition, these models can precisely and more completely describe the post-peak stress-strain behavior.

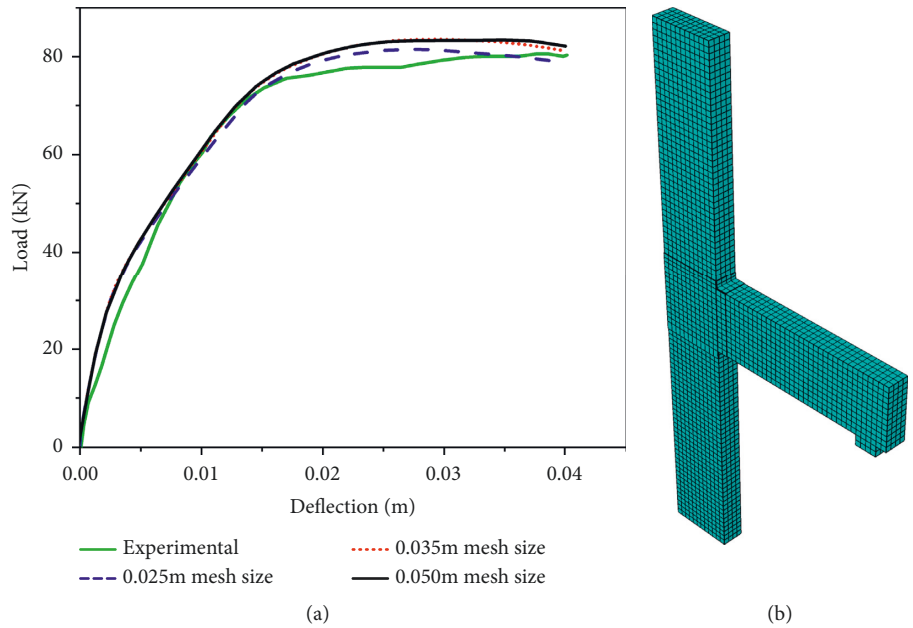


Figure 4: Delineation of the mesh: (a) comparison of different mesh sizes with experimental result and (b) finite element mesh size of 0.025.

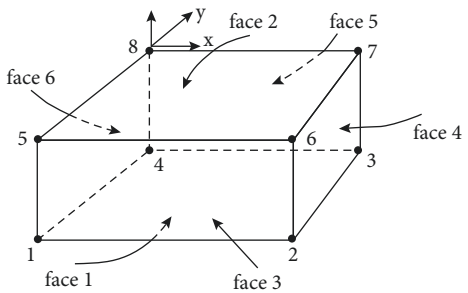


Figure 5: Eight-node brick element.

Table 1: CDPM parameters.

| Material | Dilation angle | Eccentricity | Stress ratio ($\sigma$ bo/$\sigma$ co) | Shape factor ($K_c$) | Viscosity |
|---|---|---|---|---|---|
| Concrete | 40 | 0.1 | 1.16 | 0.5 | 0.03 |

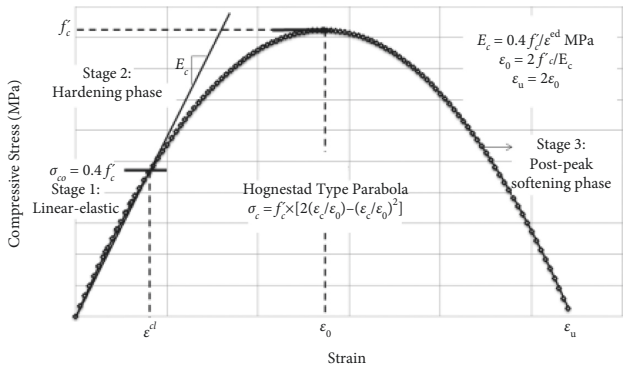


Figure 6: Hognestad pre- and post-peak parabolic concrete compression response [26].

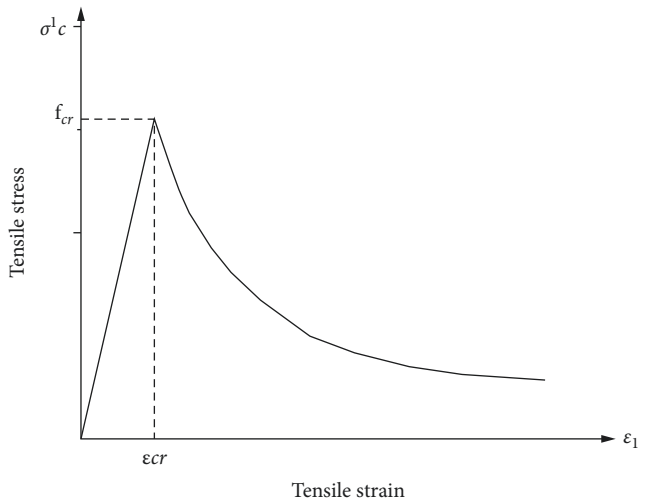


Figure 7: Tensile stress-strain curve of concrete [27].

The Hognestad [26] uniaxial stress-strain behavior of concrete can be categorized into three main domains. The first is a linear-elastic branch that continues to reach the stress level of $\sigma_{co}$, which is defined as $\sigma_{co} = 0.4\,f'c$. The second stage depicts the concrete uniaxial compressive stress-strain behavior hardening, which describes the ascending branch of the stress-strain relationship that leads to the peak load at the corresponding strain level of $\varepsilon_0 = 2f'c/\mathrm{Ec}$. The final part of the concrete uniaxial compressive stress-strain relationship represents the onset and progression of compressive damage in the concrete material until the ultimate compressive strain $\varepsilon_u$.

The tensile behavior of the concrete is defined by using the formula recommended by Belarbi and Hsu [27].

For ascending branch ($\varepsilon_1 \leq \varepsilon_{cr}$)

$$\sigma_c^1 = \mathrm{Ec} * \varepsilon_1, \quad (2)$$

where [27] Ec is the modulus of elasticity of concrete, taken as 3875 $\sqrt{\mathrm{f'c}}$, where fc′ and $\sqrt{\mathrm{f'c}}$ are in MPa; $\varepsilon_{cr}$ is the cracking strain of concrete.

For descending branch ($\varepsilon_1 > \varepsilon_{cr}$)

$$\sigma_c^1 = \mathrm{fcr}\left(\frac{\varepsilon\mathrm{cr}}{\varepsilon_1}\right)^4, \quad (3)$$

where $f_{cr}$ is cracking stress of concrete, taken as 0.31 $\sqrt{f'c}$ MPa.

*2.5.2. Reinforcement Bars.* Truss elements with two nodes and three translation degrees of freedom (T3D2) at each node are used to model steel rebars. The FE model incorporates the longitudinal and transverse steel reinforcement rebar behavior as an elastic-plastic material with a bilinear stress-strain curve as shown in Figure 8. Up to yield, the steel was assumed to be linear elastic, with a Young's modulus equal to 200 GPa and a Poisson ratio equal to 0.3.

*2.5.3. Textile Reinforced Cement.* The TRC material's behavior is characterized by a macroscopic stress-strain relationship from the test results provided by Cuypers and Wastiels [29]. In the elastic range, the material was assumed to be linearly elastic with a Young modulus of 18 GPa and a Poisson ratio of 0.3, while in the plastic range, the concrete damage plasticity (CDP) model was employed. As shown in Figure 9, after reaching the tensile strength (60 MPa), an artificial steep softening branch is added to the curve to facilitate failure simulation. The curve was designed to meet the following paradoxical requirements: it had to drop in stiffness dramatically to indicate failure, but it also had to be smooth, allowing convergence even at strains greater than the failure strain.

A macroscopic 3D finite element approach, which considers the composite TRC with its macro trilinear stress-strain relation under tensile solicitation, is adopted throughout this study to model TRC. The CDPM parameters shown in Table 2 are used throughout this study to model TRC.

## 3. Finite Element Model Validation

The experimental test results obtained by Mahmoud et al. [25] for the reference specimen and base control specimen were validated using nonlinear finite element (FE) software, in terms of load-displacement curve and crack pattern.

*3.1. Reference Specimen, JI0 Group #1.* As shown in Figure 10, from the numerical result, the behavior was linear up to a load of 64.03 kN with an associated deflection of 0.015 m, after which nonlinearity was initiated. In the nonlinear portion of the curve, the specimen has reached a maximum ultimate load of 68.49 kN with an associated displacement of 0.022 m. The load-displacement curve from the experimental program of literature indicates a yield load of 61.6 kN with an associated deflection of 0.012 m and an ultimate load

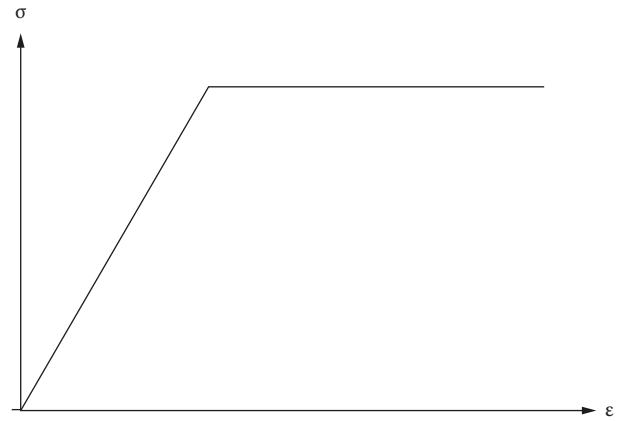


Figure 8: Idealization of the steel stress-strain curve [28].

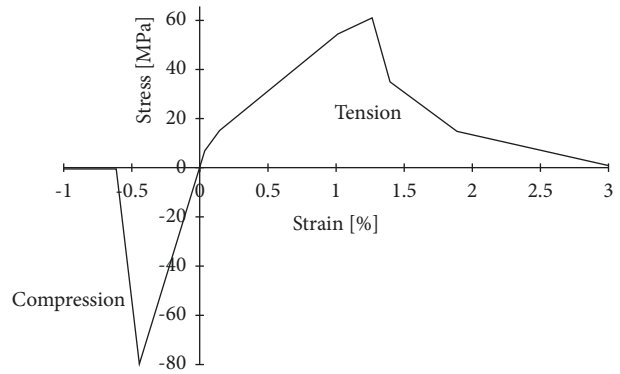


Figure 9: Stress-strain diagram of TRC in tension and compression implemented in ABAQUS.

Table 2: CDPM parameters.

| Material | Dilation angle | Eccentricity | Stress ratio ($\sigma$ bo/$\sigma$ co) | Shape factor ($K_c$) | Viscosity |
|---|---|---|---|---|---|
| TRC | 40 | 0.1 | 1.16 | 0.5 | 0.0005 |

of 67.38 kN with a corresponding ultimate deflection of 0.029 m. A summary of the load-displacement response of numerical and experimental results of the reference specimen is described in Table 3.

*3.1.1. Crack Pattern.* Experimental and finite element results of the aforementioned reference beam-column joints indicate the occurrence of crack concentration around the joint area, starting from early loading steps and propagating towards the column front face. In addition, as indicated in Figure 11, web cracks develop on the beam and then gradually follow an inclined slope.

*3.2. Control Specimen, J0*

*3.2.1. Load-Displacement Result.* As shown in Figure 12, from the numerical result, the behavior was linear up to a load of 72.12 kN with an associated deflection of 0.014 m,

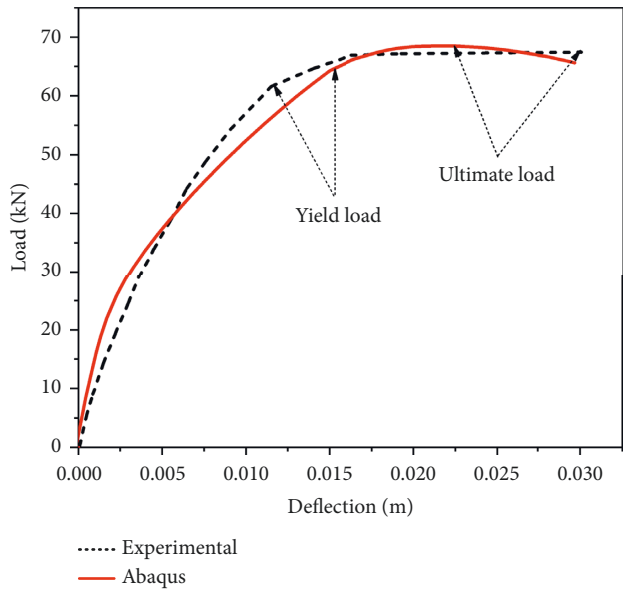


Figure 10: Comparison of the load-displacement response of the FEM and the experimental results of the reference specimen at the beam-free end.

Table 3: Summary of numerical and experimental load-deflection results for the reference specimen.

| Description | Load (kN) | | Deflection at ultimate load (m) | Deflection at yield load (m) | Percentage difference with respect to experimental | | | |
|---|---|---|---|---|---|---|---|---|
| | | | | | Load | | Deflection | |
| | Ultimate load | Yield load | | | Ultimate | Yield | At ultimate | At yield |
| Experimental | 67.38 | 61.6 | 0.029 | 0.012 | 1.65 | 3.90 | 24.13 | 25.00 |
| FEM | 68.49 | 64.03 | 0.022 | 0.015 | | | | |

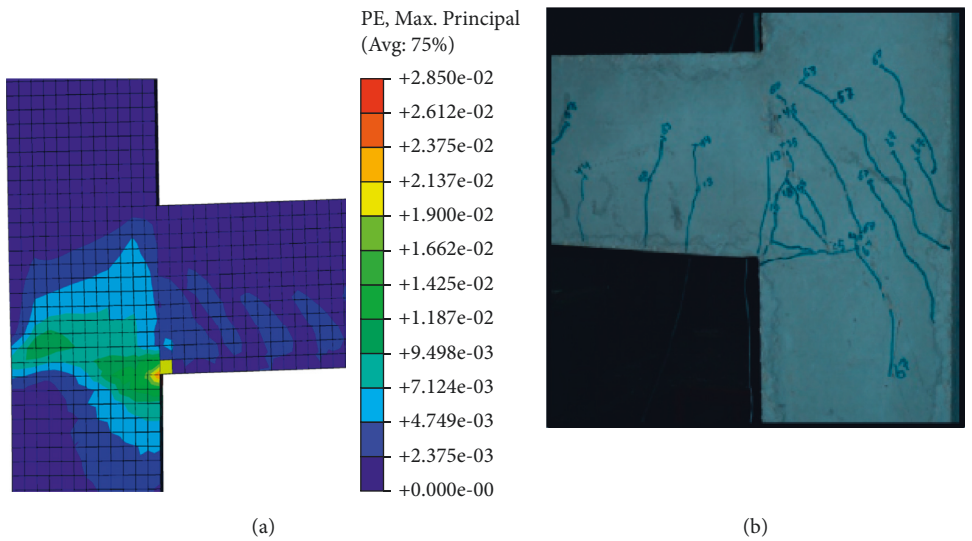


Figure 11: Crack observed at failure load: (a) FEM and (b) experimental test [25].

after which nonlinearity was initiated. In the nonlinear portion of the curve, the specimen has reached a maximum ultimate load of 81.46 kN with an associated displacement of 0.028 m. The load-displacement response from the experimental program of literature indicates a yield load of 70.45 kN with an associated deflection of 0.013 m and an ultimate load of 80.55 kN with a corresponding ultimate deflection of 0.038 m (Table 4).

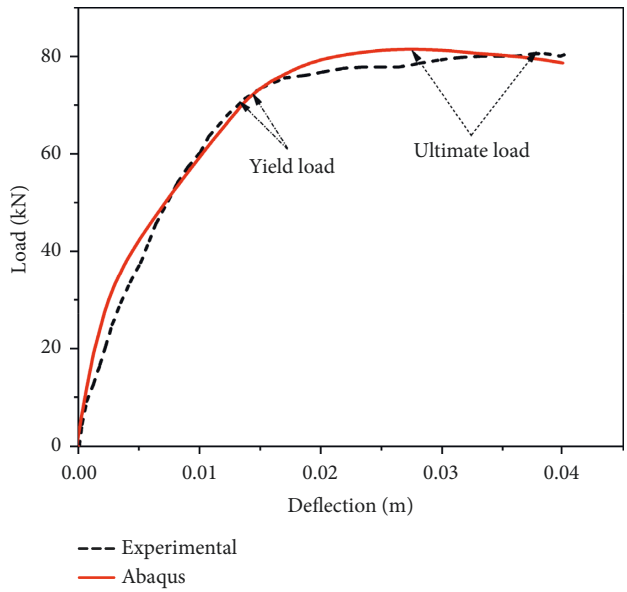


Figure 12: Comparison of the load-displacement response of the FEM and the experimental results of the control specimen at the beam-free end.

Table 4: Summary of numerical and experimental load-deflection results for control specimen.

| Description | Load (kN) | | Deflection at ultimate load (m) | Deflection at yield load (m) | Percentage difference with respect to experimental | | | |
|---|---|---|---|---|---|---|---|---|
| | | | | | Load | | Deflection | |
| | Ultimate load | Yield load | | | Ultimate | Yield | At ultimate | At yield |
| Experimental | 80.55 | 70.45 | 0.038 | 0.013 | 1.13 | 2.40 | 26.32 | 7.70 |
| FEM | 81.46 | 72.12 | 0.028 | 0.014 | | | | |

As observed, both experimental and finite element results exhibit similar behavior in terms of load-bearing capacity and failure pattern.

## 4. Textile Reinforced Cement Designed as Shear Reinforcement for Beam-Column Joint

In this numerical investigation, the load-bearing behavior of the control beam-column joint, having a conventional stirrup at the joint, and the composite beam-column joint, having TRC stay-in-place formwork as shear reinforcement at the joints, are compared to each other. Figure 13 shows the numerical load-deflection curve of the fully steel reinforced beam-column joint and the TRC shear reinforced beam-column joint. As shown in Figure 13, the start of the yielding behavior of the composite beam-column (73 kN) corresponds well to the conventional beam-column joint (72 kN). A similar correlation can be observed at the ultimate load with only a 3.7% difference, 84 kN in the case of the composite beam-column joint and 81 kN in the case of the conventional beam-column joint. This discrepancy is due to the external TRC reinforcement's contribution to the bending resistance of the beam-column. This impact is first ignored in the composite beam-column since the thickness of this external reinforcement is calculated to fulfill shear demands, but the longitudinal reinforcement is kept fixed. The finding of this study is that the TRC SiP formwork of the beam-column joint has the potential to replace conventional shear reinforcement at the joint.

## 5. Parametric Study

In this research, a parametric study involving 22 beam-column joints was carried out using the finite element package ABAQUS and the numerical model described in Table 5. The following key parameters are taken into account: the effect of an axial load, the effect of concrete compressive strength, the effect of beam longitudinal tensile reinforcement ratio, the effect of TRC thicknesses, and the effect of the presence of joint stirrup reinforcement ratio.

### 5.1. Results and Discussion

*5.1.1. Effect of an Axial Load.* In this study, five different levels of column axial load ($0.1fc'Ag$, $0.133fc'Ag$, $0.26fc'Ag$, $0.3fc'Ag$, and $0.6fc'Ag$) were investigated, and the results obtained from the software for the different performance indicators under consideration are indicated.

*(1) Shear Strength.* Table 6 shows the shear strength (represented by the maximum principal tensile stress) obtained from column axial loads of $0.1fc'Ag$, $0.133fc'Ag$, $0.26fc'Ag$, $0.3fc'Ag$, and $0.6fc'Ag$. Based on the findings of this analysis, it is reasonable to conclude that column axial load less than

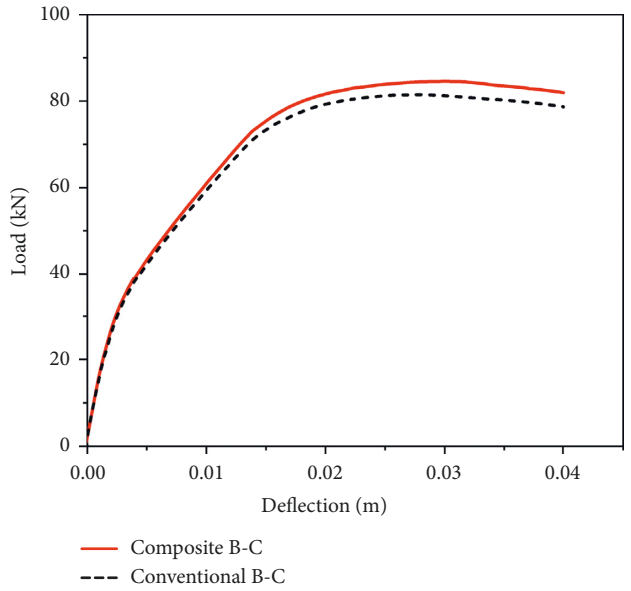


Figure 13: Comparison of load-displacement responses of conventional and composite beam-column joints at the beam-free end.

Table 5: Parametric study database and model designation.

| Group | Model | Long. reinf (beam) | Stirrup reinf. at joint | Comp. strength (MPa) | Thickness of TRC ($10^{-3}$m) | Axial force (kN) |
|---|---|---|---|---|---|---|
| *Effect of axial force* | | | | | | |
| G1 | G1M0 | 3$\phi$16 at bottom and 2$\phi$12 at top | No stirrup | 25 | 3 | Null |
| | G1M1 | 3$\phi$16 at bottom and 2$\phi$12 at top | No stirrup | 25 | 3 | 0.1f′cAg (150) |
| | Referential | 3$\phi$16 at bottom and 2$\phi$12 at top | No stirrup | 25 | 3 | 0.13f′cAg (200) |
| | G1M2 | 3$\phi$16 at bottom and 2$\phi$12 at top | No stirrup | 25 | 3 | 0.26f′cAg (400) |
| | G1M3 | 3$\phi$16 at bottom and 2$\phi$12 at top | No stirrup | 25 | 3 | 0.3f′cAg m (450) |
| | G1M4 | 3$\phi$16 at bottom and 2$\phi$12 at top | No stirrup | 25 | 3 | 0.6f′cAg (900) |
| *Effect of concrete compressive strength* | | | | | | |
| G2 | G2M1 | 3$\phi$16 at bottom and 2$\phi$12 at top | No stirrup | 15 | 3 | 200 |
| | G2M2 | 3$\phi$16 at bottom and 2$\phi$12 at top | No stirrup | 20 | 3 | 200 |
| | Referential | 3$\phi$16 at bottom and 2$\phi$12 at top | No stirrup | 25 | 3 | 200 |
| | G2M3 | 3$\phi$16 at bottom and 2$\phi$12 at top | No stirrup | 35 | 3 | 200 |
| | G2M4 | 3$\phi$16 at bottom and 2$\phi$12 at top | No stirrup | 40 | 3 | 200 |
| | G2M5 | 3$\phi$16 at bottom and 2$\phi$12 at top | No stirrup | 50 | 3 | 200 |
| *Effect of beam tensile reinforcement ratio* | | | | | | |
| G3 | G3M1 | 0.9% | No stirrup | 25 | 3 | 200 |
| | G3M2 | 1.2% | No stirrup | 25 | 3 | 200 |
| | Referential | 1.6% | No stirrup | 25 | 3 | 200 |
| | G3M3 | 2.4% | No stirrup | 25 | 3 | 200 |
| | G3M4 | 3% | No stirrup | 25 | 3 | 200 |
| | G3M5 | 4.8% | No stirrup | 25 | 3 | 200 |
| *Effect of thickness of TRC* | | | | | | |
| G4 | G4M0 | 3$\phi$16 at bottom and 2$\phi$12 at top | No stirrup | 25 | — | 200 |
| | Referential | 3$\phi$16 at bottom and 2$\phi$12 at top | No stirrup | 25 | 3 | 200 |
| | G4M1 | 3$\phi$16 at bottom and 2$\phi$12 at top | No stirrup | 25 | 6 | 200 |
| | G4M2 | 3$\phi$16 at bottom and 2$\phi$12 at top | No stirrup | 25 | 10 | 200 |
| | G4M3 | 3$\phi$16 at bottom and 2$\phi$12 at top | No stirrup | 25 | 20 | 200 |
| *Effect of joint stirrup reinforcement ratio* | | | | | | |
| G5 | Referential | 3$\phi$16 at bottom and 2$\phi$12 at top | Null | 25 | 3 | 200 |
| | G5M1 | 3$\phi$16 at bottom and 2$\phi$12 at top | 0.85% | 25 | 3 | 200 |
| | G5M2 | 3$\phi$16 at bottom and 2$\phi$12 at top | 2% | 25 | 3 | 200 |

Table 6: Shear strength response of specimens with different axial load ratios.

| Specimen description | Magnitude of load, kN | Axial load ratio | Shear strength (MPa) | Increase in shear strength with respect to G1M0 (%) | Decrease in shear strength with respect to G1M0 (%) |
|---|---|---|---|---|---|
| G1M0 | Null | Null | 16.27 | — | — |
| G1M1 | 150 | 0.1 | 16.29 | 0.12 | — |
| Referential | 200 | 0.133 | 16.18 | — | 0.55 |
| G1M2 | 400 | 0.26 | 11.49 | — | 29.68 |
| G1M3 | 450 | 0.3 | 10.7 | — | 34.23 |
| G1M4 | 900 | 0.6 | 8.67 | — | 46.68 |

Table 7: Summary of load-deflection response of specimens with different axial load ratios.

| Specimen description | Axial load ratio | Load (kN) | | | Deflection at ultimate load ($10^{-3}$m) | Deflection at yield load ($10^{-3}$ m) | Increase in ultimate load (%) with respect to G1M0 | Increase in yield load (%) with respect to G1M0 |
|---|---|---|---|---|---|---|---|---|
| | | Ultimate load | Yield load | Cracking load | | | | |
| G1M0 | Null | 65.94 | 54.9 | 19 | 36.39 | 13.29 | — | — |
| G1M1 | 0.1 | 80.27 | 70.54 | 29 | 30.14 | 14.84 | 21.72 | 28.49 |
| Referential | 0.133 | 84.57 | 73.29 | 30 | 30.30 | 15.22 | 28.27 | 33.50 |
| G1M2 | 0.26 | 94.68 | 89.18 | 39 | 27.72 | 16.43 | 43.58 | 62.44 |
| G1M3 | 0.3 | 96.68 | 90.00 | 40 | 27.05 | 14.99 | 46.60 | 63.93 |
| G1M4 | 0.6 | 102.78 | 92.33 | 53 | 26.75 | 11.65 | 55.87 | 68.18 |

0.1fc′Ag increases joint shear capacity due to confinement against shear failure, whereas column axial load greater than 0.1fc′Ag decreases joint shear capacity due to crushing of concrete and bond deterioration between rebar and surrounding concrete in the joint region caused by higher axial load. As indicated, column axial load corresponding to 0.1fc′Ag shows a positive effect on the joint shear strength, but an axial load greater than 0.1fc′Ag shows a detrimental effect on the joint shear strength. A similar conclusion is made by Pantelides et al. [8], in which the range of column axial load/axial strength ratio considered to increase joint shear capacity is very narrow and it is usually less than 0.15.

*(2) Load-Deflection*. Table 7 indicates a summary of the load-displacement response of specimens obtained using finite element software. As observed in Figure 14, with an increase in axial compression ratio, the ultimate load, yield load, and first cracking load have greatly improved, while the ultimate displacement has decreased significantly. This may be attributed to the fact that the higher axial load confined the joint against failure.

*(3) Ductility*. Ductility can be described as the ability of the material to be plastically deformed without fracture. In this study, the displacement ductility of a specimen is determined by the following equation:

$$\mu = \frac{\Delta u}{\Delta y}. \tag{4}$$

The displacement ductility factor in this case is determined according to Park et al. [30], where the yield displacement ($\Delta y$) is the displacement at 85% of ultimate load at the ascending part of the curve, while the failure displacement ($\Delta u$) is the displacement at 85% of ultimate load at the descending part of the curve. As observed from Table 8, it is reasonable to conclude that an increase in axial compression ratio up to 0.26 decreases the ductility of joint specimens, and the ductility coefficient keeps on increasing with an increase in axial load ratio beyond 0.26.

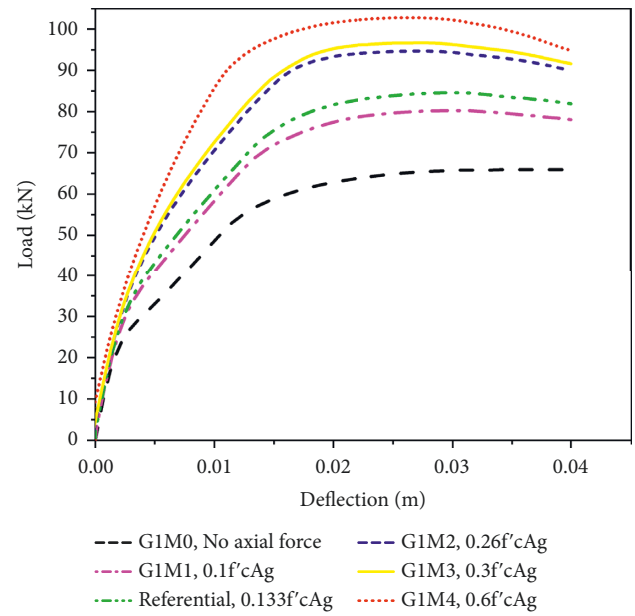


Figure 14: Load-deflection response of specimens with different axial load ratios.

*(4) Crack Pattern*. The initial fracture occurred at the bottom interface of the beam-column joint in a specimen with an

Table 8: Yield and ultimate displacement for ductility determination.

| Model | Axial load ratio | Yield displacement ($10^{-3}$m) | Ultimate displacement ($10^{-3}$m) | Ductility ($\mu$) |
|---|---|---|---|---|
| G1M0 | Null | 12.71 | 40 | 3.15 |
| G1M1 | 0.1 | 13.80 | 40 | 2.89 |
| Referential | 0.133 | 14.14 | 40 | 2.82 |
| G1M2 | 0.26 | 13.29 | 40 | 3.00 |
| G1M3 | 0.3 | 12.90 | 40 | 3.10 |
| G1M4 | 0.6 | 10.49 | 40 | 3.81 |

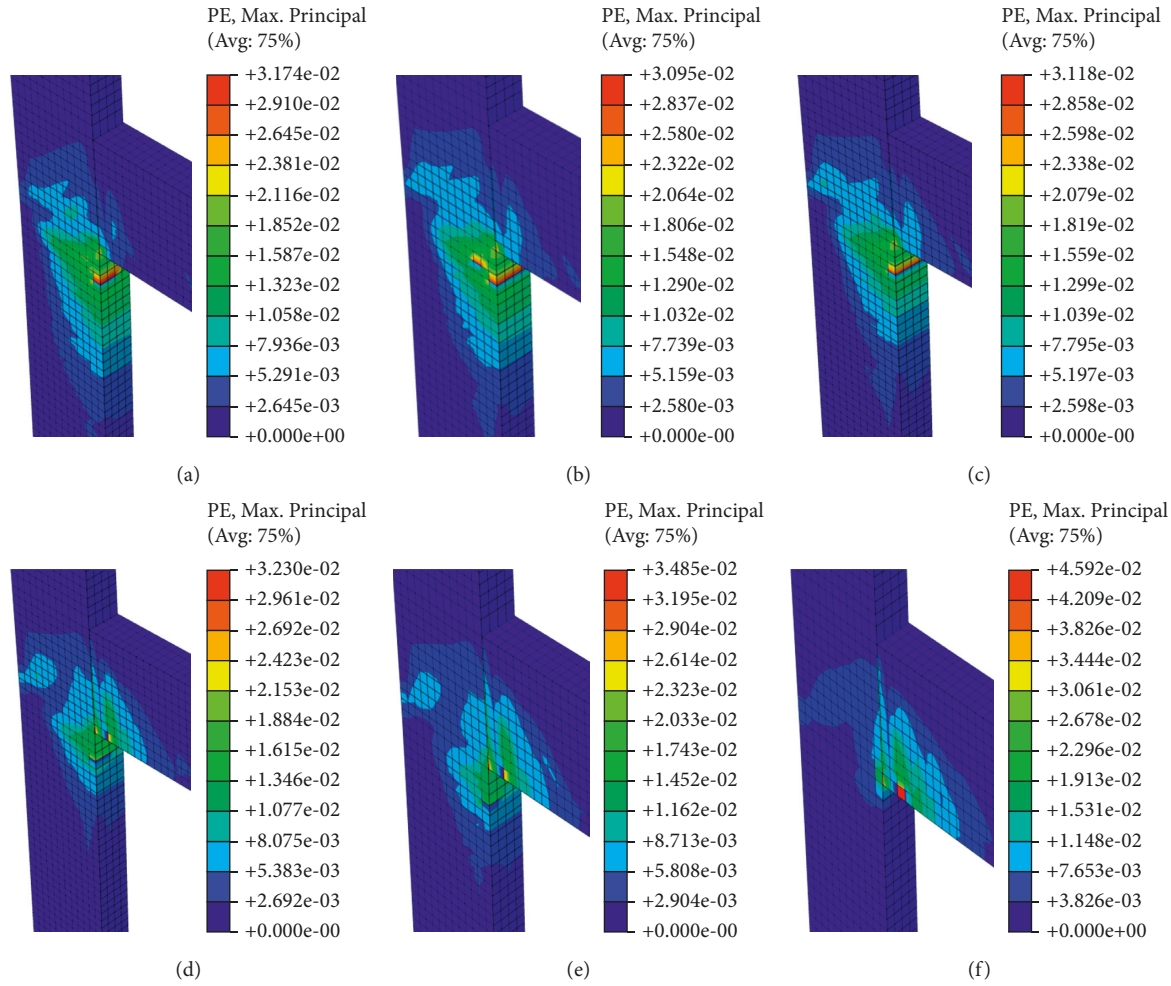


Figure 15: Crack pattern for specimens with various axial load ratios: (a) G1M0, no axial force; (b) G1M1, 0.1; (c) Referential, 0.133; (d) G1M2, 0.26; (e) G1M3, 0.3; and (f) G1M4, 0.6.

axial load of 0–0.133 f′cAg (Figure 15), and subsequently spread towards the outer edge of the column in an upward direction, yielding an inclination of 45°. In a specimen with an axial load of 0.26f′cAg–0.6f′cAg, the first crack appeared at the bottom interface of the beam-column joint and propagated in an upward direction, giving an inclination of 90°, and a very fine crack was further extended in a downward direction towards the outer edge of the column, giving an inclination of 45°. In addition, with an increase in axial load ratio, the crack location has changed from the inside of the joint to the beam-column joint's face, which may be attributed to an increase in ductility beyond 0.26 axial load ratio. The finding of this parametric study is that a higher axial load ratio changes the failure mode from joint brittle shear failure to beam ductile flexural failure. It is also observed that higher axial load increases the inclination of main diagonal shear cracks.

*(5) Concrete Compression Damage.* As can be seen from Figure 16, an increase in axial load ratio results in the failure of the joint concrete in shear compression. This may be attributed to the fact that a higher axial load ratio deteriorates

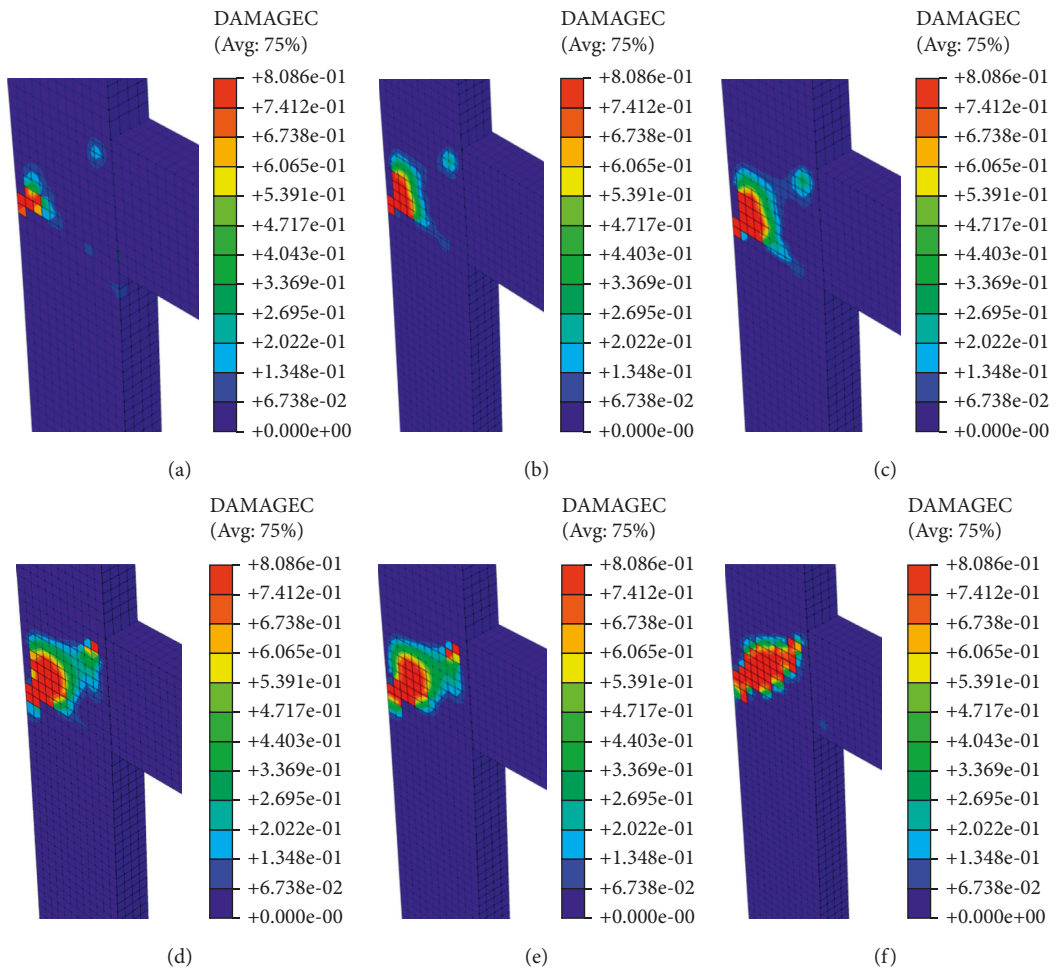


Figure 16: Concrete compression damage for specimens with various axial load ratios: (a) G1M0, no axial force; (b) G1M1, 0.1; (c) Referential, 0.133; (d) G1M2, 0.26; (e) G1M3, 0.3; and (f) G1M4, 0.6.

Table 9: Shear strength response of specimens with different compressive strengths.

| Specimen description | Compressive strength (MPa) | Shear strength (MPa) | Increase (%) in shear strength with respect to G2M1 |
|---|---|---|---|
| G2M1 | 15 | 8.37 | — |
| G2M2 | 20 | 14.4 | 72.04 |
| Referential | 25 | 16.18 | 93.31 |
| G2M3 | 35 | 20.62 | 146.36 |
| G2M4 | 40 | 20.86 | 149.22 |

Table 10: Load-deflection response of specimens with different concrete strengths.

| Specimen description | Concrete strength (MPa) | Load (kN) | | | Deflection at ultimate load ($10^{-3}$m) | Deflection at yield load ($10^{-3}$ m) | Increase in ultimate load with respect to G2M1 (%) | Increase in yield load with respect to G2M1 (%) |
|---|---|---|---|---|---|---|---|---|
| | | Ultimate load | Yield load | Cracking load | | | | |
| G2M1 | 15 | 71.77 | 67.08 | 24.06 | 23.56 | 16.27 | — | — |
| G2M2 | 20 | 80.27 | 71.95 | 26.91 | 26.83 | 15.02 | 11.84 | 7.26 |
| Referential | 25 | 84.58 | 73.02 | 30.60 | 30.29 | 14.84 | 17.84 | 8.86 |
| G2M3 | 35 | 93.13 | 82.20 | 33.29 | 31.39 | 14.26 | 29.76 | 22.54 |
| G2M4 | 40 | 98.70 | 87.76 | 37.60 | 33.96 | 13.85 | 37.52 | 30.83 |
| G2M5 | 50 | 103.01 | 91.40 | 40.00 | 36.84 | 13.31 | 43.52 | 36.26 |

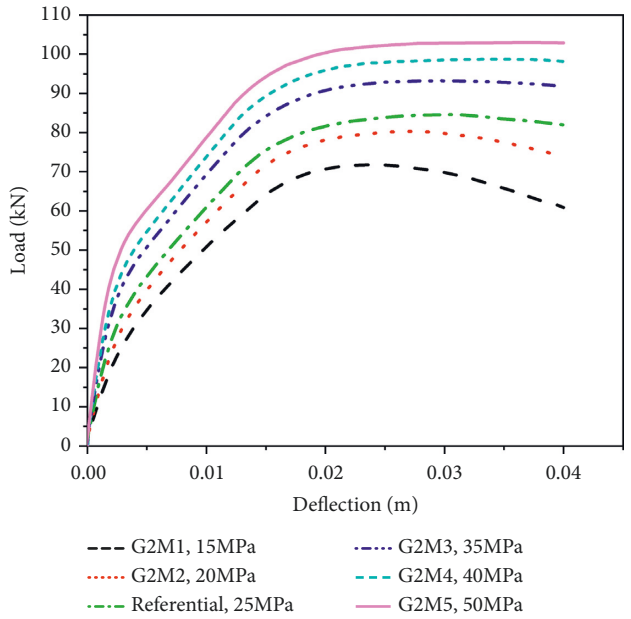


Figure 17: Load-deflection response for specimens with various concrete compressive strengths.

Table 11: Yield and ultimate displacement for ductility determination.

| Model | Compressive strength (MPa) | Yield displacement ($10^{-3}$m) | Ultimate displacement ($10^{-3}$m) | Ductility ($\mu$) |
|---|---|---|---|---|
| G2M1 | 15 | 15.40 | 40 | 2.60 |
| G2M2 | 20 | 14.40 | 40 | 2.77 |
| Referential | 25 | 14.14 | 40 | 2.83 |
| G2M3 | 35 | 13.04 | 40 | 3.07 |
| G2M4 | 40 | 12.38 | 40 | 3.23 |
| G2M5 | 50 | 11.90 | 40 | 3.36 |

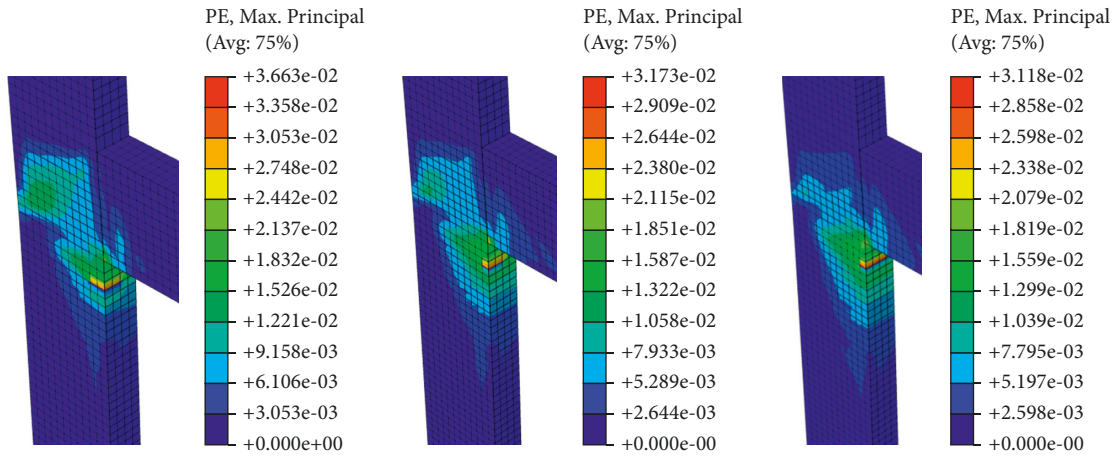


Figure 18: Continued.

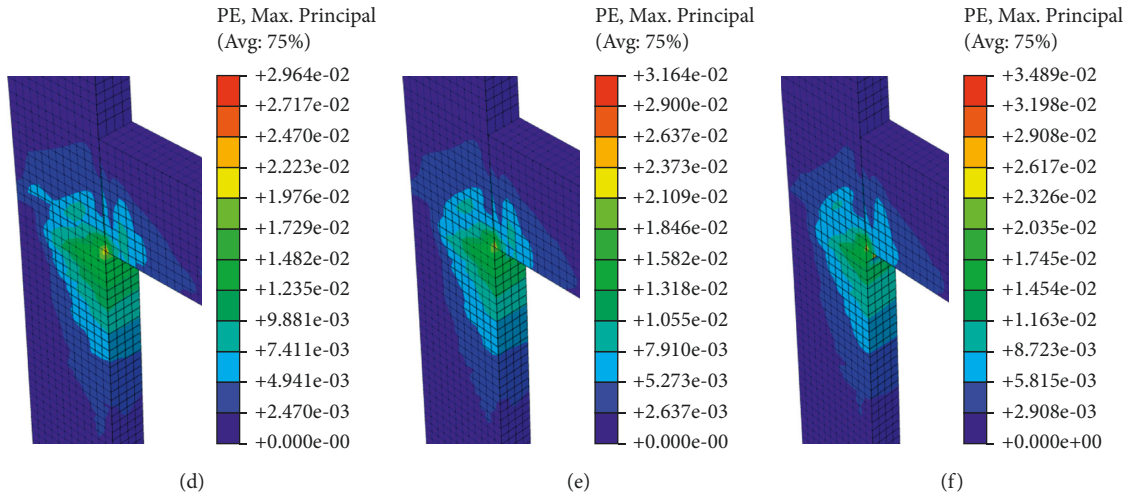


Figure 18: Crack pattern for specimens with various concrete compressive strengths: (a) G2M1, 15 MPa; (b) G2M2, 20 MPa; (c) Referential, 25 MPa; (d) G2M3, 35 MPa; (e) G2M4, 40 MPa; and (f) G2M5, 50 MPa.

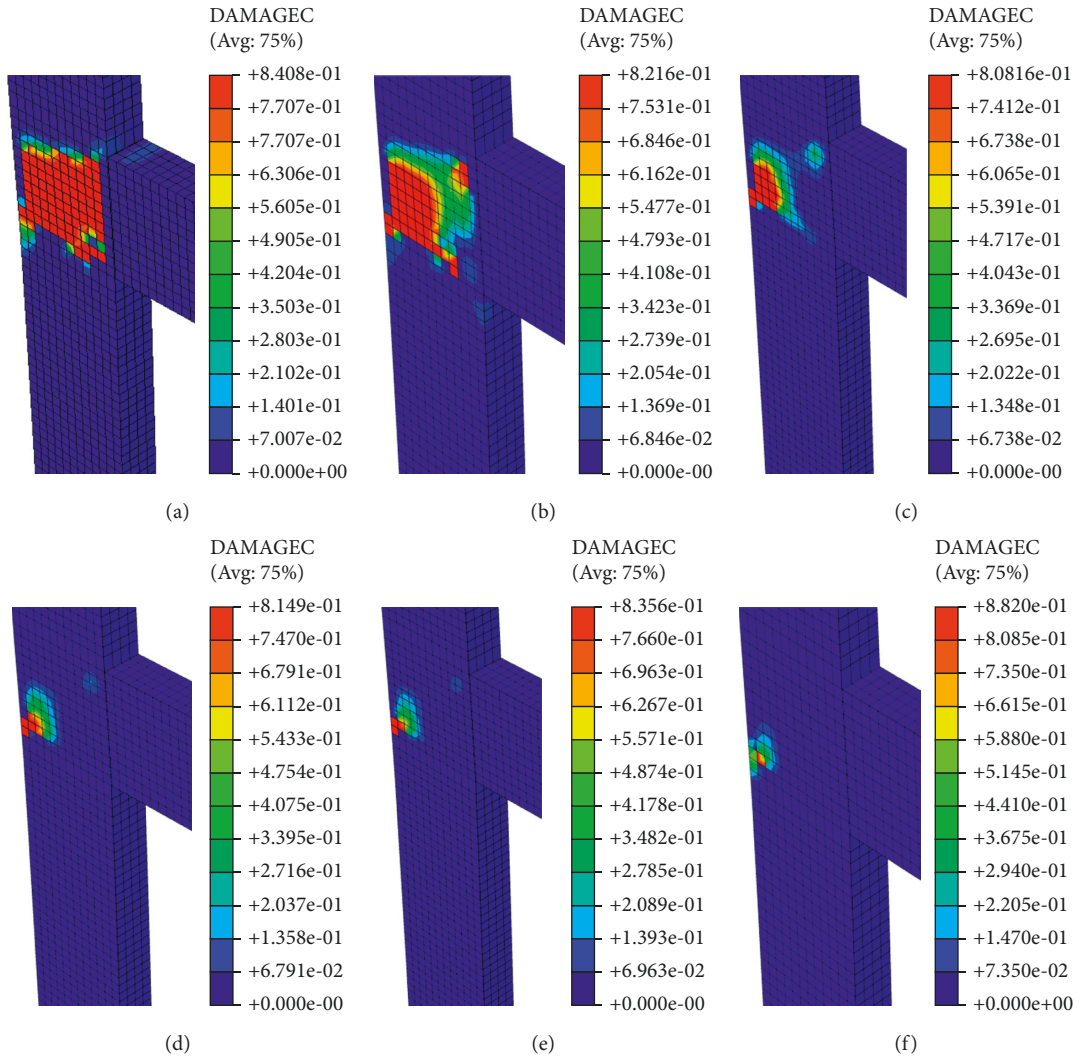


Figure 19: Concrete compression damage of specimens with various compressive strengths: (a) G2M1, 15 MPa; (b) G2M2, 20 MPa; (c) Referential, 25 MPa; (d) G2M3, 35 MPa; (e) G2M4, 40 MPa; and (f) G2M5, 50 MPa.

the bond along the beam reinforcement after yielding. Distribution cloud pictures of the compressive damage indicate that, for the specimens with a high axial load ratio, in the late loading stage, the compressive damage area increases.

*5.1.2. Effect of Concrete Compressive Strength.* To observe the effect of the compressive strength of concrete on the performance of the beam-column joint, different strengths of concrete (15 MPa, 20 MPa, 25 MPa, 35 MPa, 40 MPa, and 50 MPa) were considered for the analysis.

*(1) Shear Strength.* As observed from Table 9, the joint shear strength (represented by the maximum principal tensile stress) changes with the variation of concrete compressive strength and increases as concrete compressive strength increases. This is attributed to the fact that increasing the concrete strength improves the joint resistance by improving the column and the beam compression zone as well as the bond strength of the beam bars within the joint region.

*(2) Load-Deflection.* Table 10 shows the load-displacement response of a specimen obtained using finite element software. As can be seen in Figure 17, with an increase in concrete compressive strength, the ultimate load, yield load, and first cracking load have greatly improved.

*(3) Ductility.* In Table 11, the ratio of the failure displacement and the yield displacement is used to express the displacement ductility coefficient. From this study, it was observed that an increase in concrete compressive strength increases the ductility of the specimens. The TRC confining reinforcement at the joint can compensate for the loss of ductility caused by the use of higher strength concrete. This will increase the ductility of the concrete beam-column by increasing the confining pressure on the concrete core. In addition, increased concrete strength reduces the neutral axis depth and raises the strain that the tension reinforcement will reach when the concrete is crushed, resulting in increased ductility at fixed tension and compression reinforcement levels.

*(4) Crack Pattern.* Figure 18 displays the crack pattern observed in specimens subjected to monotonic loading at failure with varying concrete strengths. The first fracture, as observed, occurred at the bottom interface of the beam-column connection and progressed upward towards the outside border of the column, giving a 45° inclination. Furthermore, from Figure 18, it was observed that with an increase in concrete compressive strength, the crack location from inside the joint has moved to the beam-column joint's face. Therefore, it is possible to conclude from this analysis that, with a further increase in concrete strength beyond 50 MPa, the failure mechanism will change from shear failure in the joint to beam flexural failure.

*(5) Concrete Compression Damage.* Figure 19 displays the distribution cloud pictures of concrete damage in compression. As observed, the beam-column joint specimen experienced crushing in the joint core and no concrete crushing was observed elsewhere. The analysis result indicated that increasing concrete's compressive strength is effective in mitigating the damage area of concrete. As a result of this analysis, it can be concluded that, in comparison to specimens with high compressive strength, the distribution of compressive damage area in the joint core is large, but the degree of compression is smaller, and the distribution for specimens with low compressive strength is more uniform.

Table 12: Shear strength response of specimens with different tensile reinforcement ratios.

| Specimen description | Tensile reinf. ratio (%) | Shear strength (MPa) | Increase (%) in shear strength with respect to G3M1 |
|---|---|---|---|
| G3M1 | 0.9 | 6.84 | — |
| G3M2 | 1.2 | 9.83 | 43.27 |
| Referential | 1.6 | 16.18 | 136.55 |
| G3M3 | 2.4 | 16.98 | 148.25 |
| G3M4 | 3 | 17.05 | 149.27 |
| G3M5 | 4.8 | 11.61 | 69.74 |

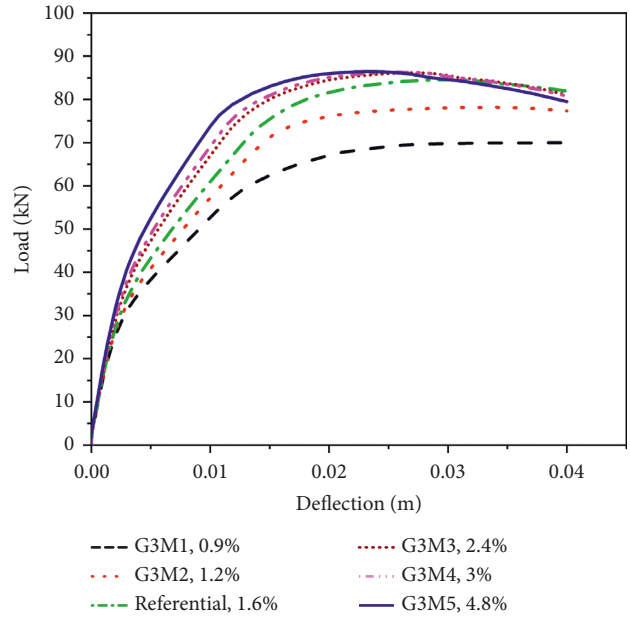


Figure 20: Load-deflection response of specimens with various tensile reinforcement ratios.

*5.1.3. Effect of Beam Tensile Reinforcement Ratio.* An analysis was conducted here to study the effect of the beam longitudinal tensile reinforcement ratio on the performance of the beam-column joint using different proposed reinforcement ratios (0.9%, 1.2%, 1.6%, 2.4%, 3%, and 4.8%).

*(1) Shear Strength.* Shear strength (represented by the maximum principal tensile stress) obtained from specimens with a reinforcement ratio of 0.9%, 1.2%, 1.6%, 2.4%, 3%,

Table 13: Load-deflection response of specimens with different tensile reinforcement ratios.

| Specimen description | Reinf. ratio (%) | Load (kN) | | | Deflection at ultimate load ($10^{-3}$ m) | Deflection at yield load ($10^{-3}$ m) | Increase in ultimate load with respect to G3M1 (%) | Increase in yield load with respect to G3M1 (%) |
|---|---|---|---|---|---|---|---|---|
| | | Ultimate load | Yield load | Cracking load | | | | |
| G3M1 | 0.9 | 70.02 | 59.55 | 25.05 | 39.96 | 12.69 | — | — |
| G3M2 | 1.2 | 78.18 | 70.87 | 27.47 | 33.70 | 14.88 | 11.65 | 19.01 |
| Referential | 1.6 | 84.58 | 73.29 | 30.60 | 30.29 | 14.84 | 20.79 | 23.07 |
| G3M3 | 2.4 | 86.16 | 75.44 | 35.37 | 26.72 | 12.79 | 23.09 | 26.68 |
| G3M4 | 3 | 86.33 | 77.52 | 39.72 | 25.70 | 12.45 | 23.29 | 30.18 |
| G3M5 | 4.8 | 86.47 | 78.70 | 41.24 | 23.36 | 11.51 | 23.49 | 32.16 |

Table 14: Yield and ultimate displacement for ductility determination.

| Model | Reinforcement ratio (%) | Yield displacement ($10^{-3}$m) | Ultimate displacement ($10^{-3}$m) | Ductility ($\mu$) |
|---|---|---|---|---|
| G3M1 | 0.9 | 13.08 | 40 | 3.06 |
| G3M2 | 1.2 | 13.48 | 40 | 2.97 |
| Referential | 1.6 | 14.14 | 40 | 2.83 |
| G3M3 | 2.4 | 12.02 | 40 | 3.33 |
| G3M4 | 3 | 11.27 | 40 | 3.55 |
| G3M5 | 4.8 | 10.01 | 40 | 4.00 |

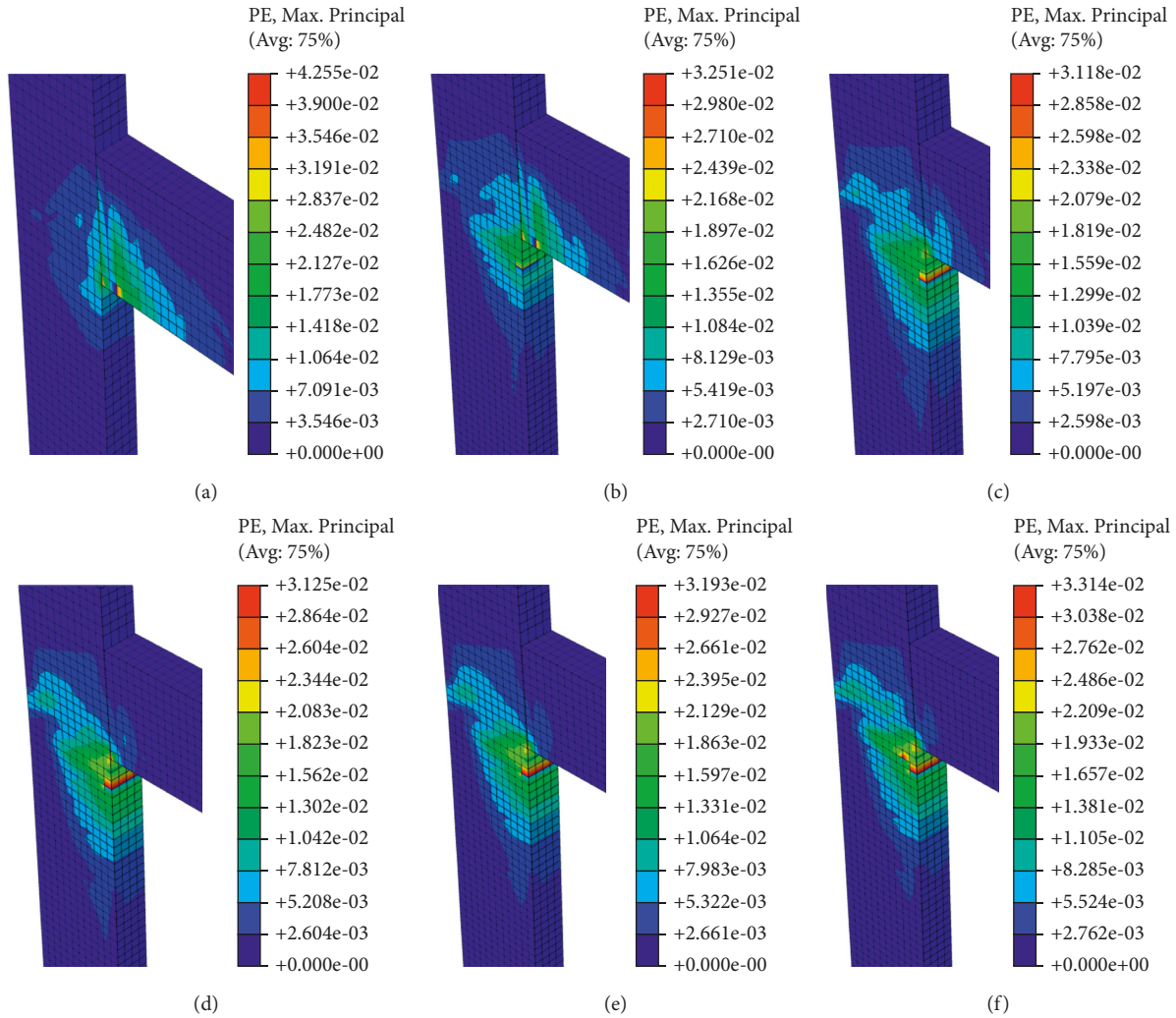


Figure 21: Crack pattern for specimens with various beam tensile reinforcement ratios: (a) G3M1, 0.9%; (b) G3M2, 1.2%; (c) Referential, 1.6%; (d) G3M3, 2.4%; (e) G3M4, 3%; and (f) G3M5, 4.8%.

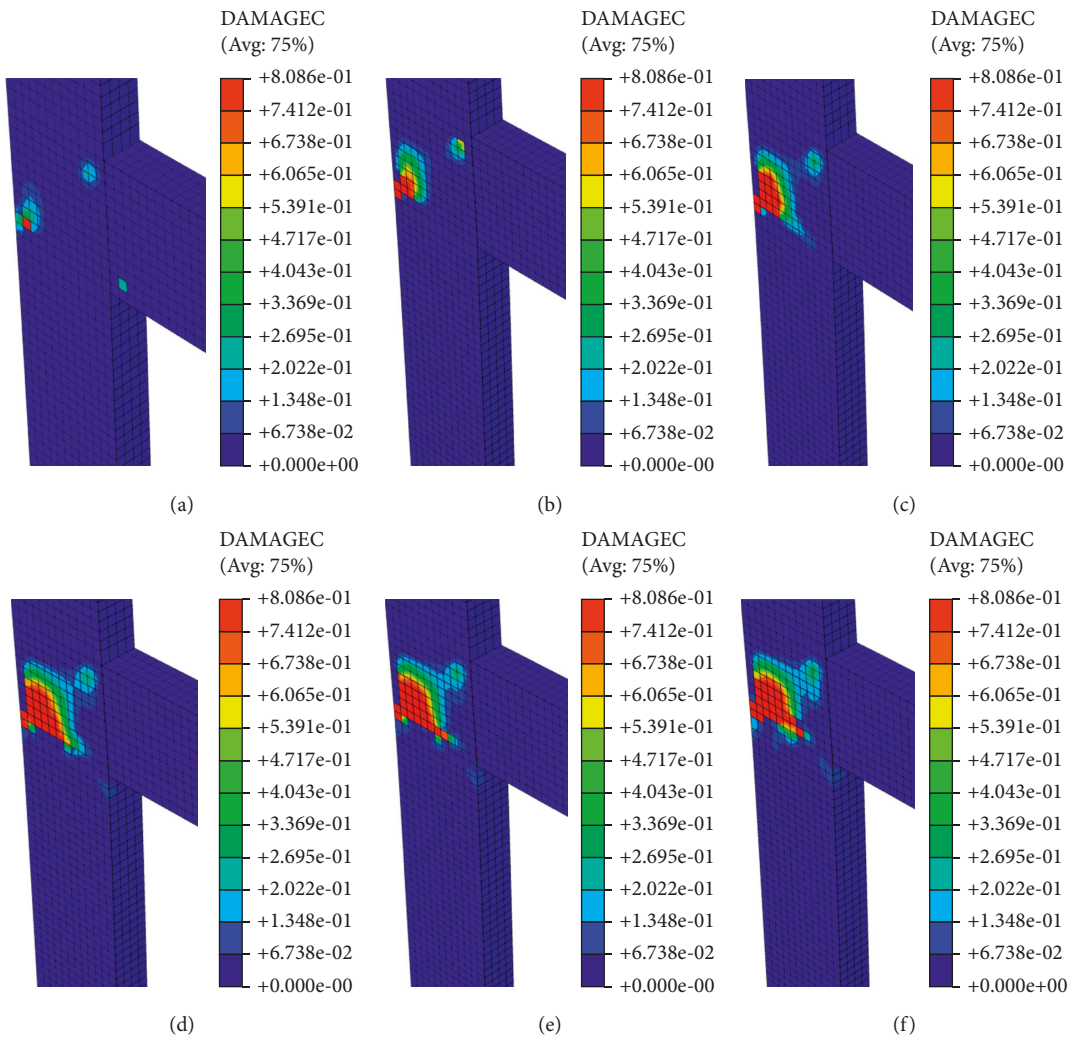


Figure 22: Concrete compression damage for specimens with various reinforcement ratios: (a) G3M1, 0.9%; (b) G3M2, 1.2%; (c) Referential, 1.6%; (d) G3M3, 2.4%; (e) G3M4, 3%; and (f) G3M5, 4.8%.

and 4.8% is shown in Table 12. As expected, the specimen with the lowest reinforcement ratio, 0.9%, exhibited the lowest shear capacity at the joint. From this analysis result, it is reasonable to conclude that increasing the reinforcement ratio up to 3% increases the shear capacity of the joint linearly. This may be due to the fact that increasing the beam reinforcement ratio enhances joint confinement and improves force transfer between the beam and the column, resulting in an increase in joint capacity. For subsequent reinforcement ratios beyond 3%, increasing reinforcement ratios decreases shear capacity. This may be attributed to the fact that a higher reinforcement ratio could lead to compression failure due to reinforcement congestion.

*(2) Load-Deflection*. The load-displacement response, Figure 20, is generated in this study to investigate the effect of the beam tensile reinforcement ratio on the performance of the beam-column joint. The analysis result in Table 13 indicated that, with an increase in reinforcement ratios up to 3%, the load-bearing capacity has greatly improved, and there is no significant load-bearing capacity increment observed beyond the reinforcement ratio of 3% at the ultimate.

*(3) Ductility*. In Table 14, the ratio of the failure displacement and the yield displacement is used to express the displacement ductility coefficient. As observed, displacement ductility coefficient decreases with an increase in tensile reinforcement ratio up to 1.6%, and for subsequent reinforcement ratios beyond 1.6%, displacement ductility coefficient keeps increasing with an increase in reinforcement ratio. An increase in ductility observed is attributed to increased strain and concrete curvature resulting from the presence of TRC confining reinforcement at the joint core. TRC confinement at the joint section helps prevent ductility loss caused by a high tensile reinforcement ratio.

*(4) Crack Pattern*. Figure 21 displays the crack pattern observed in specimens having different beam tensile reinforcement ratios subjected to monotonic loading at failure. In specimens with a reinforcement ratio of 0.9% and 1.2%, the first crack appeared at the bottom face of the

Table 15: Shear strength response of specimens with different thicknesses of TRC.

| Specimen description | Thickness of TRC ($10^{-3}$m) | Shear strength (MPa) | Increase (%) in shear strength with respect to G4M0 |
|---|---|---|---|
| G4M0 | — | 7.07 | — |
| Referential | 3 | 7.52 | 6.36 |
| G4M1 | 6 | 8.72 | 23.34 |
| G4M2 | 10 | 10.53 | 48.94 |

Table 16: Load-deflection response of specimens with different thicknesses of TRC.

| Specimen description | TRC thickness ($10^{-3}$m) | Load (kN) | | | Deflection at ultimate load ($10^{-3}$m) | Deflection at yield load ($10^{-3}$m) | Increase in ultimate load with respect to G4M0 (%) | Increase in yield load with respect to G4M0 (%) |
|---|---|---|---|---|---|---|---|---|
| | | Ultimate load | Yield load | Cracking load | | | | |
| G4M0 | — | 81.01 | 70.28 | 26.50 | 26.42 | 13.47 | — | — |
| Referential | 3 | 84.58 | 73.29 | 30.60 | 30.29 | 14.84 | 4.41 | 4.28 |
| G4M1 | 6 | 85.42 | 74.15 | 32.54 | 31.43 | 13.73 | 5.44 | 5.51 |
| G4M2 | 10 | 86.42 | 75.71 | 34.07 | 34.96 | 13.96 | 6.68 | 7.73 |
| G4M3 | 20 | 87.92 | 76.85 | 36.81 | 38.15 | 13.44 | 8.53 | 9.35 |

beam-column joint, giving an inclination of 90°, followed by a beam flexural crack. In subsequent specimens with reinforcement ratios of 1.6%, 2.4%, 3%, and 4.8%, the initial fracture occurred at the bottom interface of the beam-column joint and propagated in an upward direction, at an inclination of 45°. Furthermore, from Figure 21, it was observed that with an increase in reinforcement ratio, the crack location from the beam has moved to the beam-column joint core. This means that the failure mechanism was changed from beam ductile flexural failure to brittle shear failure at the joint core.

*(5) Concrete Compression Damage*. As observed from Figure 22, the beam-column joint specimen experienced crushing in the joint core and no concrete crushing was observed elsewhere. From the numerical results also, it can be observed that with an increase in reinforcement ratio, the concrete compression damage cloud picture was increased gradually, but the degree of compression remained the same in all cases. This is due to the fact that increasing the tensile reinforcement ratio of a beam cross section shifts the neutral axis in the direction of the tension area, resulting in a larger extent of concrete compression area being utilized. This condition enlarges the compression area of the concrete cross section to be damaged. As a result, specimens with a higher reinforcement ratio will experience greater damage area than specimens with a lower reinforcement ratio.

*5.1.4. Effect of Thickness of Textile Reinforced Cement (TRC).* The effect of the thickness of TRC on the performance of the beam-column joint is investigated in this study using five different thicknesses: (Control -Zero thickness of TRC, 0.003 m, 0.006 m, 0.01 m, and 0.02 m).

*(1) Shear Strength*. The maximum principal tensile stresses obtained from specimens with a thickness of 0.003 m, 0.006 m, 0.01 m, and without TRC are depicted in Table 15. The numerical value of maximum principal tensile stress in this study is taken from the same element for comparison. As expected, the specimen without TRC at the joint core exhibited the lowest shear capacity. It was found from the analysis results that increasing the thickness of TRC generally increases the shear capacity of the member. This is due to the fact that increasing the thickness of the TRC enhances joint confinement and improves force transfer between the beam and the column, resulting in an increase in the member's capacity.

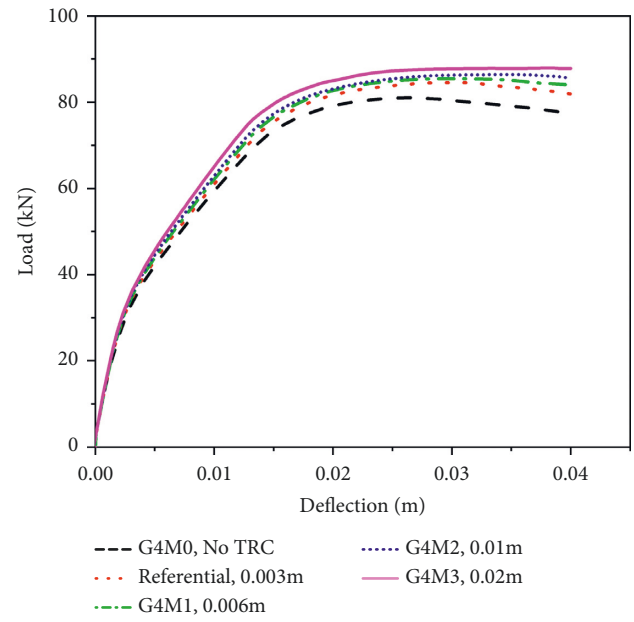


Figure 23: Load-deflection response of specimens with different thicknesses of TRC.

*(2) Load-Deflection*. Table 16 depicts a summary of the numerical analysis result of the performance of a beam-column joint with different thicknesses of TRC in terms of

Table 17: Yield and ultimate displacement for ductility determination.

| Model | Thickness of TRC ($10^{-3}$m) | Yield displacement ($10^{-3}$m) | Ultimate displacement ($10^{-3}$m) | Ductility ($\mu$) |
|---|---|---|---|---|
| Referential | 3 | 14.14 | 40 | 2.83 |
| G4M1 | 6 | 13.54 | 40 | 2.95 |
| G4M2 | 10 | 13.31 | 40 | 3.00 |
| G4M3 | 20 | 12.71 | 40 | 3.15 |

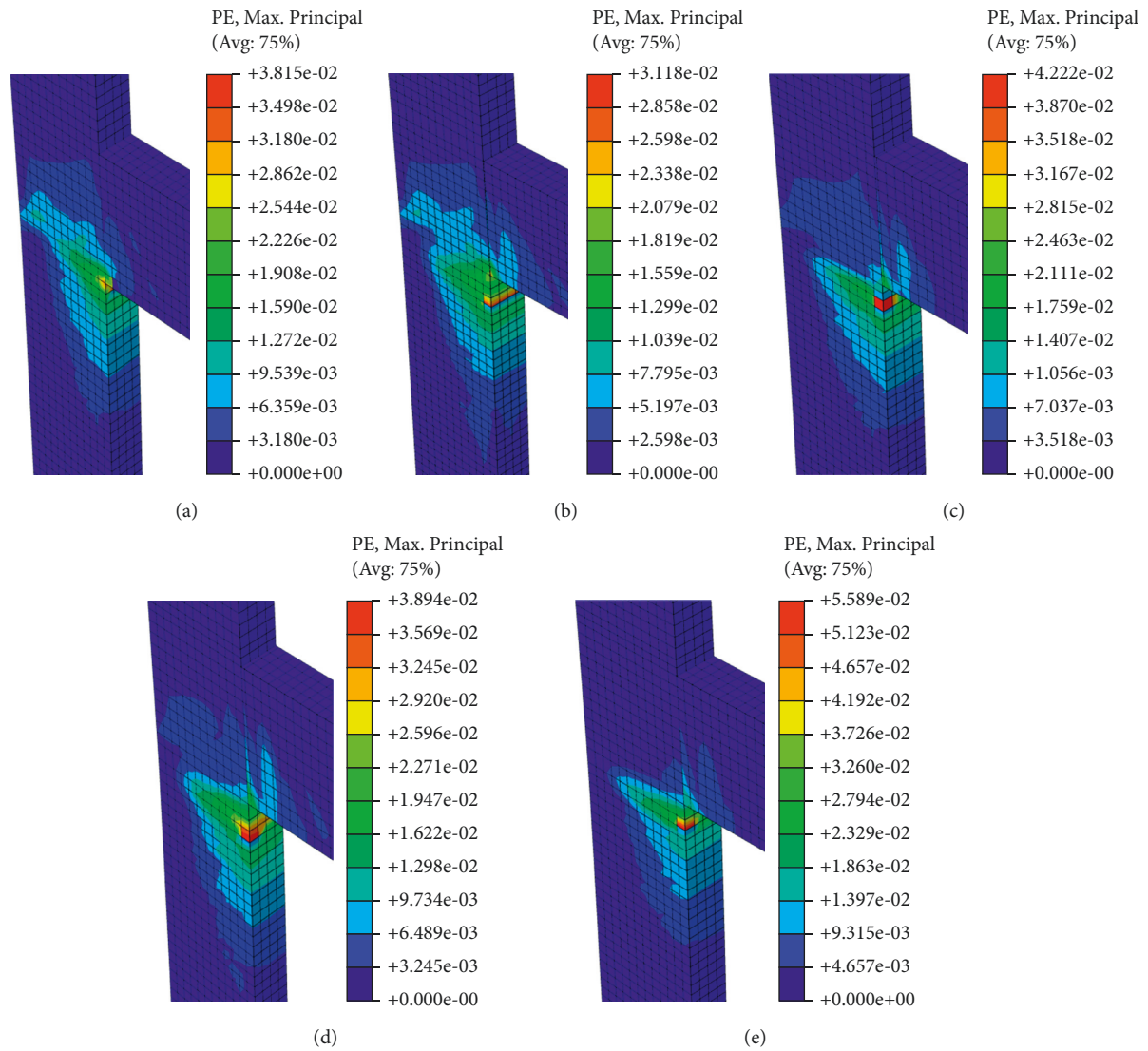


Figure 24: Crack pattern for specimens with various thicknesses of TRC: (a) G4M0, without TRC; (b) Referential, 0.003 m; (c) G4M1, 0.006 m; (d) G4M2, 0.01 m; and (e) G4M3, 0.02 m.

load-deflection response. As indicated in Figure 23, an increase in load-bearing capacity was observed with an increase in the thickness of TRC at both ultimate and yield.

*(3) Ductility*. To observe the effects of the thickness of TRC on the ductility of the beam-column joint, different thicknesses of TRC as presented in Table 17 are considered for analysis. As can be seen, the ductility of the beam-column joint changes with the variation of the thickness of TRC and increases as TRC thickness increases.

*(4) Crack Pattern*. Figure 24 displays the crack pattern observed in specimens subjected to monotonic loading at failure with varying thicknesses of TRC. The first crack occurred at the bottom interface of the beam-column joint in a specimen with a TRC thickness of 0.003 m and no TRC at the joint, and then propagated upward towards the outer

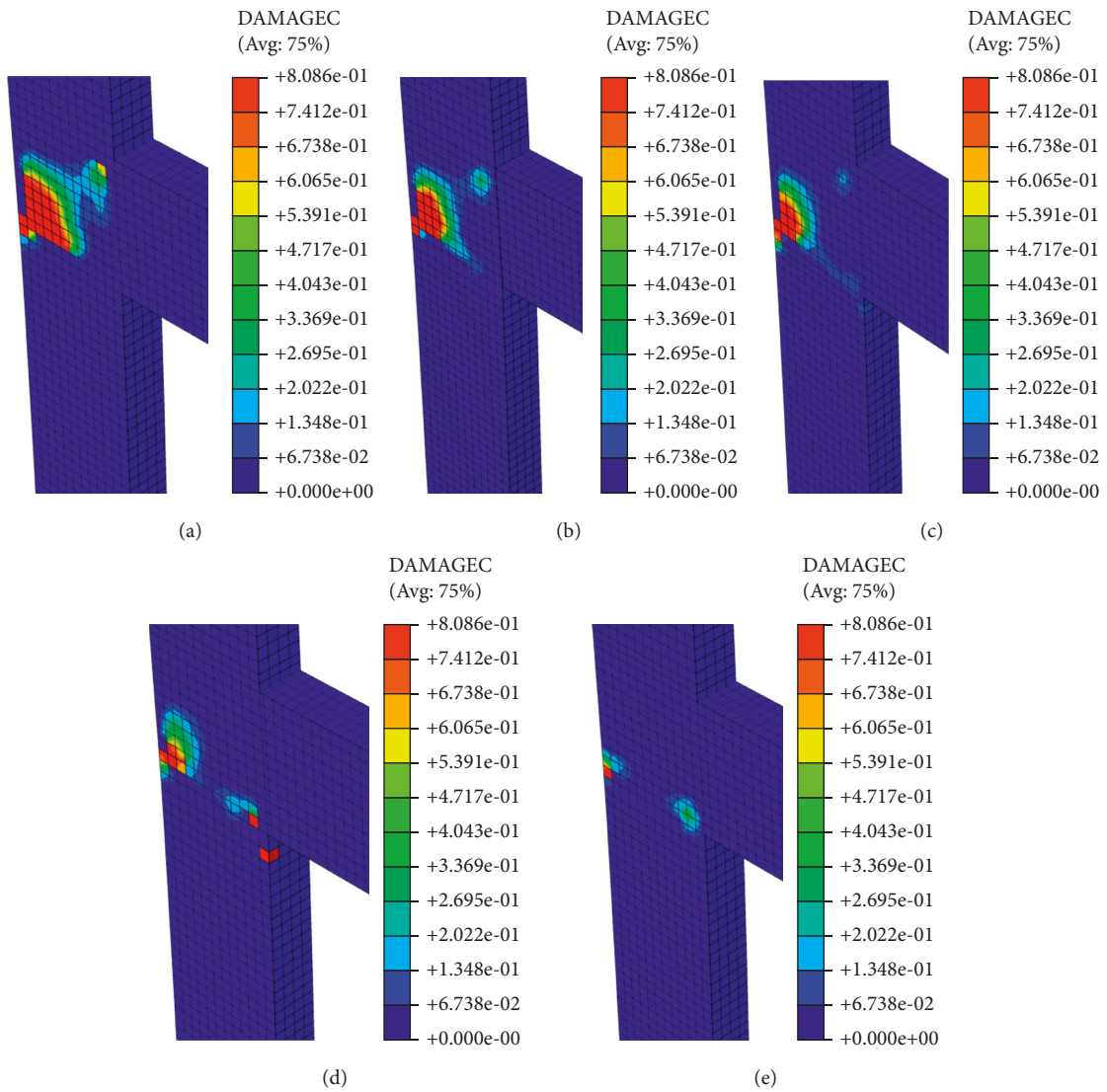


Figure 25: Concrete compression damage for specimens with various thicknesses of TRC: (a) G4M0, without TRC; (b) Referential, 0.003 m; (c) G4M1, 0.006 m; (d) G4M2, 0.01 m; and (e) G4M3, 0.02 m.

edge of the column at a 45° inclination. The crack pattern has changed significantly as the TRC thickness has been increased to 0.02 m. The crack location shifted from the inside of the joint core to the column member in specimens with TRC thicknesses of 0.006 m and 0.01 m, and a very fine crack developed at the bottom interface of the beam-column joint and propagated upward at an inclination of 45°. In a subsequent specimen with a TRC thickness of 0.02 m, the crack location totally shifted from the inside of the joint to the column member. This means that the failure mechanism has changed from joint shear failure to column flexural tension failure. Generally, from this analysis result, it is reasonable to conclude that an increase in the thickness of TRC changes the failure mechanism from brittle joint shear failure to ductile column flexural tension failure.

*(5) Concrete Compression Damage.* Figure 25 displays the distribution cloud pictures of concrete damage in compression for specimens having TRC thicknesses of 0.003 m, 0.006 m, 0.01 m, and 0.02 m. As observed from Figure 25, the beam-column joint specimen experienced crushing in the joint core and no concrete crushing was observed elsewhere. The results of the numerical analysis indicated that increasing the thickness of TRC is effective in mitigating the damage area of the joint core. Compared to the specimen with the smaller thickness of TRC, the distribution of compressive damage area of the specimen with the larger TRC thickness on the joint is gradually decreased, but the degree of compression remains the same. This finding is attributed to the fact that, in comparison with the smaller thickness of TRC, the larger thickness of TRC effectively restrains core concrete and decreases its swelling deformation, thereby reducing the damage area of the joint concrete section.

*5.1.5. Effect of Joint Stirrup Reinforcement Ratio.* The influence of joint stirrup reinforcement ratio on the

Table 18: Shear strength response of specimens with different stirrup reinforcement ratios.

| Specimen description | Stirrup reinf. ratio | Shear strength (MPa) | Increase (%) in shear strength with respect to referential |
|---|---|---|---|
| Referential | Null | 16.18 | — |
| G5M1 | 0.85% | 16.42 | 1.48 |
| G5M2 | 2% | 16.54 | 2.22 |

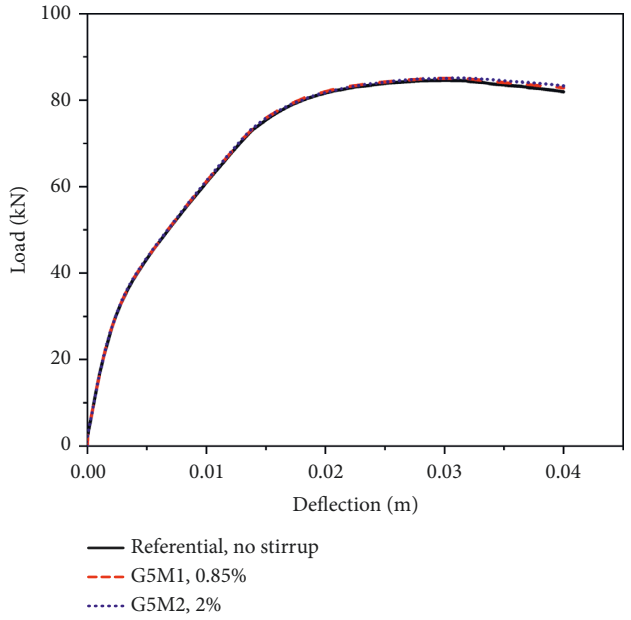


Figure 26: Load-deflection response of specimens with different joint stirrup ratios.

Table 19: Load-deflection response of specimens with different joint stirrup ratios.

| Specimen description | Stirrup reinf. ratio | Load (kN) | | | Deflection at ultimate load ($10^{-3}$ m) | Deflection at yield load ($10^{-3}$ m) | Increase in ultimate load with respect to referential (%) | Increase in yield load with respect to referential (%) |
|---|---|---|---|---|---|---|---|---|
| | | Ultimate load | Yield load | Cracking load | | | | |
| Referential | Null | 84.58 | 73.29 | 30.60 | 30.29 | 14.84 | — | — |
| G5M1 | 0.85% | 85.02 | 73.60 | 30.93 | 31.00 | 13.93 | 0.52 | 0.42 |
| G5M2 | 2% | 85.10 | 74.10 | 31.30 | 31.6 | 13.99 | 0.61 | 1.1 |

performance of beam-column joints was investigated in this study based on the joint core having stirrup reinforcement ratios of 0.85% and 2%.

*(1) Shear Strength*. The effect of the joint stirrup reinforcement ratio on shear strength is presented in Table 18. This analysis result indicated that increasing stirrup reinforcement ratio at the joint has a limited effect on the shear strength of the beam-column joint, provided proper confinement is maintained at the joint. This may be attributed to the fact that textile reinforced cement provided as external confining reinforcement at the joint core may reduce the effectiveness of the stirrup in enhancing the shear capacity of the joint. This result is reasonable according to the study carried out by Taylor [31], in which the presence of the joint shear reinforcement (ties) did not lead to any significant enhancement in the joint shear capacity.

*(2) Load-Deflection*. A numerical investigation was performed in this study to investigate the effect of the joint vertical stirrup reinforcement ratio on the load-bearing capacity of the beam-column joint. In this study, the load-displacement curve, Figure 26, is generated for beam-column joints having joint stirrup reinforcement ratios of 0.85% and 2%, and a comparison is made with respect to the joint core without shear reinforcement. Table 19 shows a summary of the load-displacement responses of specimens with different joint stirrup reinforcement ratios, obtained using finite element software. The results indicated that increasing the joint stirrup reinforcement ratio has no or limited effect on load-bearing capacity, provided proper confinement is maintained at the joint. This is briefly discussed by Kamimura et al. [19], in which experimental test results indicated that the amount of shear reinforcement in the joint had little influence on the strength and deformation of beam-column connections.

Table 20: Yield and ultimate displacement for ductility determination.

| Model | Joint stirrup ratio | Yield displacement ($10^{-3}$m) | Ultimate displacement ($10^{-3}$m) | Ductility ($\mu$) |
|---|---|---|---|---|
| Referential | Null | 14.14 | 40 | 2.83 |
| G5M1 | 0.85% | 13.96 | 40 | 2.87 |
| G5M2 | 2% | 13.91 | 40 | 2.88 |

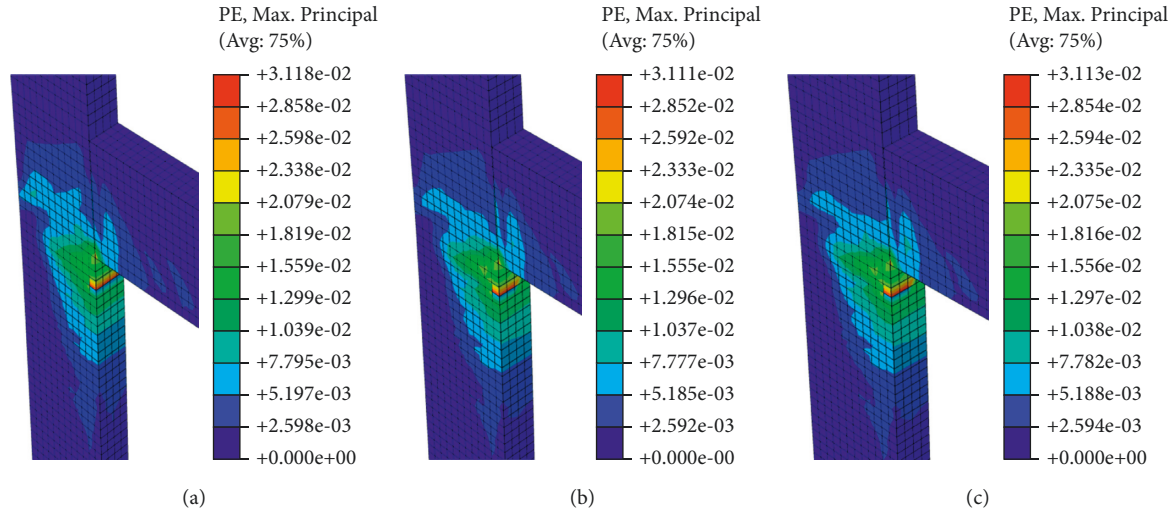


Figure 27: Crack pattern for specimens with different joint stirrup reinforcement ratios: (a) Referential, no shear reinforcement; (b) G5M1, 0.85%; and (c) G5M2, 2%.

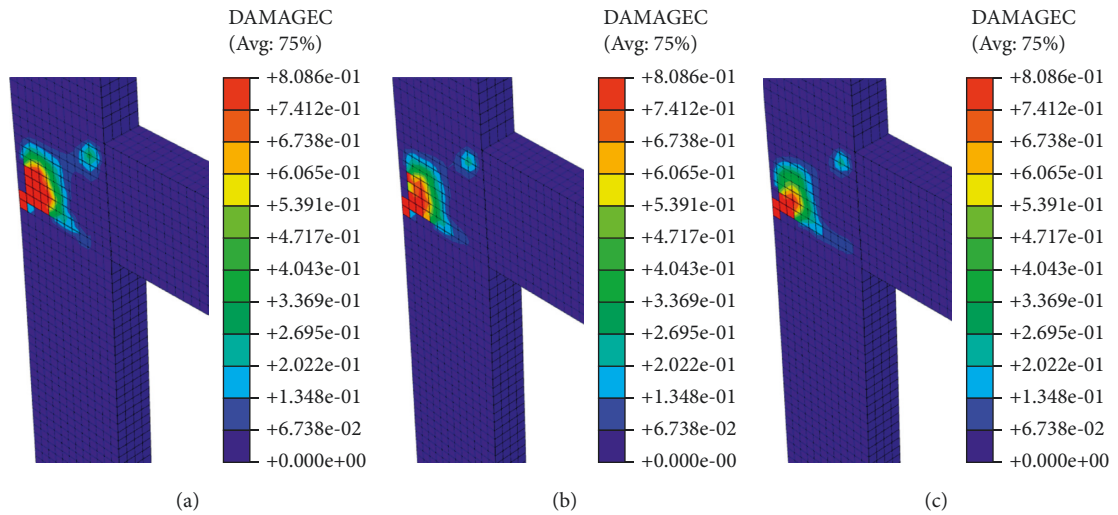


Figure 28: Concrete compression damage for specimens with different joint stirrup ratios: (a) Referential, no shear reinforcement; (b) G5M1, 0.85%; and (c.) G5M2, 2%.

*(3) Ductility*. In Table 20, the ratio of the failure displacement and the yield displacement is used to express the displacement ductility coefficient. The analysis result indicated that the ductility of the beam-column joint increases with an increase in the joint stirrup reinforcement ratio, but not significantly, provided proper confinement is maintained at the joint.

*(4) Crack Pattern*. As observed in Figure 27, the crack pattern in each specimen was essentially similar. The first crack occurred at the bottom interface of the beam-column joint and propagated in an upward direction. This crack was typically located near the center of the core and approximately along the diagonal direction. The cracks emerged at the end of the beam near the joint as well, and the cracks at the end of the beam developed slowly. The vertical reinforcement across the joint region has no evident influence on the cracking strength of joints as indicated in the load-deflection curve, but it affects the distribution and width of

cracks in the joint region. As can be observed from Figure 27, compared to a specimen without a joint stirrup, the crack width in a specimen with joint reinforcement ratios of 0.85% and 2% is small. This is attributed to the fact that the presence of joint shear reinforcement restricts crack propagation and slows the loss in confinement, thereby reducing the rate of bond degradation.

*(5) Concrete Compression Damage*. Figure 28 displays the distribution cloud pictures of concrete damage in compression for specimens having joint stirrup reinforcement ratios of 0.85% and 2%. From this analysis, it is possible to conclude that stirrups have a restraint effect on the concrete in the joint region. The restraint effect of stirrups was more obvious in the specimen with a joint stirrup reinforcement ratio of 2%. It can be seen from the distribution cloud pictures of the compressive damage in Figure 28 that for the specimens with a low stirrup reinforcement ratio, in the late loading stage, the compressive damage area increases. This finding is observed because, in a specimen with a low stirrup reinforcement ratio, the stirrup fails to effectively restrain the core concrete's swelling deformation, thereby increasing the damage area of the joint concrete.

## 6. Conclusions

(i) The FE models developed using ABAQUS were able to predict the load-displacement response and failure mode, as they closely matched the respective experimental results.

(ii) The start of the composite beam-column yielding behavior corresponds well to the conventional beam-column joint. There is only a 3.7% difference at ultimate load. The finding of this investigation indicates that SiP formwork of TRC designed as shear reinforcement for beam-column joints exhibits similar yielding behavior to fully steel stirrup reinforced beam-column joints, such that TRC SiP formwork has the potential to be used as shear reinforcement at the joint.

(iii) When compared to a beam-column joint with no axial load ratio, shear strength increased by 0.12% for beam-column joints with an axial load ratio of 0.1 and decreased by 46.68% for beam-column joints with an axial load ratio of 0.6. The range of column axial load/axial strength ratio considered to increase joint shear capacity is very narrow and is less than 0.1. Increasing the concrete strength from 15 MPa to 40 MPa resulted in an increase in shear strength by 149.22%. There was an increment in shear strength by 149.27% with an increase in beam tensile reinforcement ratio from 0.9% to 3%, and increasing the reinforcement ratio above 3% rapidly decreases the strength of the joint. The shear strength of a joint with a TRC thickness of 10 mm was increased by 48.94% compared to a joint with no TRC, whereas the joint stirrup ratio had little effect.

(iv) Increasing the axial compression ratio from null to 0.6 increased the ultimate, yield, and first cracking load by 55.87%, 68.18%, and 178.95%, respectively. When compared to a joint with a compressive strength of 15 MPa, the ultimate, yield, and first cracking load of a beam-column joint with a compressive strength of 50 MPa increased by 43.52%, 36.26%, and 66.25%, respectively. The ultimate, yield, and first cracking load of the joint in the range of tensile reinforcement ratio from 0.9% to 4.8% were found to be increased with the tensile reinforcement ratio, whereas the joint shear reinforcement ratio and thickness of TRC have only a little influence.

(v) Increasing the axial load ratio from null to 0.26 and the tensile reinforcement ratio from 0.9% to 1.6% decreased ductility, whereas an increase in the strength of concrete, thickness of TRC, and joint stirrup ratio enhanced ductility.

(vi) A higher axial load ratio changes the failure mode from joint brittle shear failure to beam ductile flexural failure, but an increase in tensile reinforcement ratio does the reverse, whereas an increase in the thickness of TRC changes the failure mode from brittle joint shear failure to ductile column flexural tension failure.

(vii) An increase in the axial load ratio and tensile reinforcement ratio increased the concrete compression damage area, but an increase in the strength of concrete, joint stirrup ratio, and thickness of TRC reduced the damage area of concrete.

## Data Availability

The data used to support the findings of this study are included within the article.

## Conflicts of Interest

The authors declare no conflicts of interest.

## Acknowledgments

This study was supported by Addis Ababa Science and Technology University, Ethiopia.

## References

[1] S. Hoon Kang, S. Gul Hong, and Y. Hee Kwon, "Effect of permanent formwork using ultra-high performance concrete on structural behaviour of reinforced concrete beam subjected to bending as a function of reinforcement parameter," *Journal of Applied Mechanical Engineering*, vol. 06, no. 02, 2017.

[2] W. Meng, K. H. Khayat, and W. Meng, "Development of stay-in-place formwork using GFRP reinforced UHPC elements," in *Proceedings of the First International Interactive Symposium on UHPC*, pp. 1–9, Missouri University of Science and Technology, Rolla, July 2016.

[3] M. Nelson and A. Fam, "Structural GFRP permanent forms with T-shape ribs for bridge decks supported by precast concrete girders," *Journal of Bridge Engineering*, vol. 18, no. 9, pp. 813–826, 2013.

[4] S. Verbruggen, O. Remy, J. Wastiels, and T. Tysmans, "Stay-in-Place formwork of TRC designed as shear reinforcement for concrete beams," *Advances in Materials Science and Engineering*, vol. 2013, pp. 1–9, Article ID 648943, 2013.

[5] S. De Sutter, O. Remy, T. Tysmans, and J. Wastiels, "Development and experimental validation of a lightweight Stay-in-Place composite formwork for concrete beams," *Construction and Building Materials*, vol. 63, pp. 33–39, 2014.

[6] S. M. Allam, H. M. Elbakry, and I. S. Arab, "Exterior reinforced concrete beam column joint subjected to monotonic loading," *Alexandria Engineering Journal*, vol. 57, no. 4, pp. 4133–4144, 2018.

[7] M. A. Al-Osta, U. Khan, M. H. Baluch, and M. K. Rahman, "Effects of variation of axial load on seismic performance of shear deficient RC exterior BCJs," *International Journal of Concrete Structures and Materials*, vol. 12, no. 1, p. 46, 2018.

[8] C. P. Pantelides, C. Clyde, and L. D. Reaveley, "Performance-based evaluation of reinforced concrete building exterior joints for seismic excitation," *Earthquake Spectra*, vol. 18, no. 3, pp. 449–480, 2002.

[9] V. G. Haach, A. Lúcia Homce De Cresce El Debs, and M. Khalil El Debs, "Evaluation of the influence of the column axial load on the behavior of monotonically loaded R/C exterior beam-column joints through numerical simulations," *Engineering Structures*, vol. 30, no. 4, pp. 965–975, 2008.

[10] S. Pantazopoulou and J. Bonacci, "Consideration of questions about beam-column joints," *ACI Structural Journal*, vol. 89, no. 1, 1993.

[11] S. Park and K. Mosalam, "Shear strength models of exterior beam-column joints without transverse reinforcement," vol. 115, 2009.

[12] K. Shi, M. Zhang, T. Zhang, P. Li, J. Zhu, and L. Li, "Seismic performance of steel fiber reinforced high-strength concrete beam-column joints," *Materials*, vol. 14, no. 12, p. 3235, 2021.

[13] Z. Yang, Y. Liu, and J. Li, "Study of seismic behavior of RC beam-column joints strengthened by sprayed FRP," *Advances in Materials Science and Engineering*, vol. 2018, pp. 1–10, Article ID 3581458, 2018.

[14] A. Masi, G. Santarsiero, A. Mossucca, and D. Nigro, "Influence of axial load on the seismic behavior of RC beam-column joints with wide beam," *Applied Mechanics and Materials*, vol. 508, pp. 208–214, 2014.

[15] H. Noguchi and T. Kashiwazaki, "Experimental studies on shear performance of RC interior column-beam joints," *In Tenth World Conference on Earthquake Engineering*, vol. 41, pp. 3163–3168, 1992.

[16] M. T. Tran, "Influence factors for the shear strength of exterior and interior reinforced concrete beam-column joints," *Procedia Engineering*, vol. 142, pp. 63–70, 2016.

[17] B. Abdelwahed, B. Belkassem, and J. Vantomme, "Reinforced concrete beam-column inverted knee joint behaviour after ground corner column loss-numerical analysis," *Latin American Journal of Solids and Structures*, vol. 15, no. 10, 2018.

[18] S. Park, "Experimental and analytical studies on old reinforced concrete buildings with seismically vulnerable beam-column joints (PhD dissertation)," *University of California, Berkeley*, vol. 20, 2010.

[19] T. Kamimura, S. Takeda, and M. Tochio, "Influence of joint reinforcement on strength and deformation of interior beam-column subassemblages," *Proceedings of the 12WCEE*, vol. 142, 2000.

[20] J. S. Kaung and H. F. Wong, "Effectiveness of horizontal stirrups in joint core for exterior beam-column joints with nonseismic design," *Procedia Engineering*, vol. 14, pp. 3301–3307, 2011.

[21] C. G. Karayannis and E. Golias, "Full-scale experimental testing of RC beam-column joints strengthened using CFRP ropes as external reinforcement," *Engineering Structures*, vol. 250, Article ID 113305, 2022.

[22] M. M. Maras and F. Kantarcı, "Structural performance of reinforced concrete (RC) moment frame connections strengthened using FRP composite jackets," *Arabian Journal for Science and Engineering*, vol. 46, no. 11, pp. 10975–10992, 2021.

[23] D. Wang, Y. Ju, W. Zheng, and H. Shen, "Seismic behavior and shear bearing capacity of ultra-high performance fiber-reinforced concrete (UHPFRC) beam-column joints," *Applied Sciences*, vol. 8, no. 5, p. 810, 2018.

[24] K. Prasanna, R. Ramasubramani, K. S. Anandh, Saisabarish, V. K. Maddu, and V. Maddu, "Strengthening of beam—column joint with steel fibre reinforced concrete under seismic loading," *IOP Conference Series: Earth and Environmental Science*, vol. 80, no. 1, Article ID 012040, 2017.

[25] M. H. Mahmoud, H. M. Afefy, N. M. Kassem, and T. M. Fawzy, "Strengthening of defected beam-column joints using CFRP," *Journal of Advanced Research*, vol. 5, no. 1, pp. 67–77, 2014.

[26] E. Hognestad, "A study of combined bending and axial load in reinforced concrete members," *Engineering Experiment Station, University of Illinois*, vol. 49, 1951.

[27] A. Belarbi and T. Hsu, "Constitutive laws of concrete in tension and reinforcing bars stiffened by concrete," *ACI Structural Journal*, vol. 91, no. 4, pp. 465–474, 1994.

[28] ASCE, "ASCE task committee on finite element analysis of reinforced concrete structures," *State-of-the-Art Report on Finite Element Analysis of Reinforced Concrete*, ASCE Special Publications, New York, 1982.

[29] H. Cuypers and J. Wastiels, "A stochastic cracking theory for the introduction of matrix multiple cracking in textile reinforced concrete under tensile loading," *In Proceedings of the 1st International RILEM Conference on Textile Reinforced Concretes*, vol. 39, pp. 193–202, 2006.

[30] R. Park, "Ductility evaluation from laboratory and analytical testing," *In Proceedings of The 9th World Conference On Earthquake Engineering*, vol. 8, pp. 605–616, 1988.

[31] H. Taylor, "The behavior of in situ concrete beam-column joints," Report 42.492, Cement and Concrete Association, London, 1974.